

The Inductive Bias of Convolutional Neural Networks: Locality and Weight Sharing Reshape Implicit Regularization

Tongtong Liang¹ Esha Singh¹ Rahul Parhi¹ Alexander Cloninger¹ Yu-Xiang Wang¹

Abstract

We study how architectural inductive bias reshapes the implicit regularization induced by the edge-of-stability phenomenon in gradient descent. Prior work has established that for fully connected networks, the strength of this regularization is governed solely by the global input geometry; consequently, it is insufficient to prevent overfitting on difficult distributions such as the high-dimensional sphere. In this paper, we show that locality and weight sharing fundamentally change this picture. Specifically, we prove that provided the receptive field size m remains small relative to the ambient dimension d , these networks generalize on spherical data with a rate of $n^{-\frac{1}{6}+O(m/d)}$, a regime where fully connected networks provably fail. This theoretical result confirms that weight sharing couples the learned filters to the low-dimensional patch manifold, thereby bypassing the high dimensionality of the ambient space. We further corroborate our theory by analyzing the patch geometry of natural images, showing that standard convolutional designs induce patch distributions that are highly amenable to this stability mechanism, thus providing a systematic explanation for the superior generalization of convolutional networks over fully connected baselines.

1. Introduction

Convolutional neural networks (CNNs) (Fukushima, 1988; LeCun et al., 2002) are among the most successful neural architectures. The renaissance of CNNs in computer vision tasks (Krizhevsky et al., 2012; Ronneberger et al., 2015; He et al., 2016) effectively ignited the modern deep learning revolution. CNNs remain a dominant choice in image and video generative models today (see, e.g., Lai et al., 2025, and the references therein).

¹University of California, San Diego. Correspondence to: Tongtong Liang <tliang@ucsd.edu>, Yu-Xiang Wang <yuxiangw@ucsd.edu>.

Preprint. March 6, 2026.

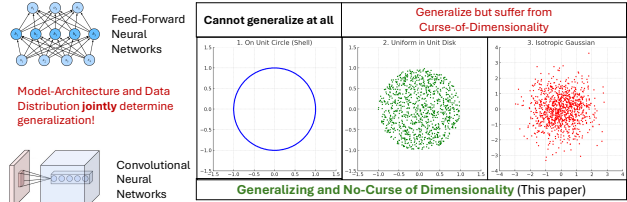


Figure 1. In the overparameterized regime, model architectures and input data distribution jointly determine the implicit regularization of gradient descent. The local patch representations of the Convolutional NNs *provably* prevent the curse-of-dimensionality in normalized / whitened distributions that break Feedforward NNs.

Modern CNN models are *overparameterized* — they are both deep (many layers) and wide (many convolutional filters) and often have more parameters than the number of data points to fit them. It was shown that, despite the ability to fit pure noise perfectly, overparameterized CNNs trained with gradient descent tend to generalize well with no explicit regularization — much more so than their densely connected counterparts (Zhang et al., 2017; Arpit et al., 2017, Figure 1). It remains a mystery how the CNN architecture interacts with the implicit bias of gradient descent that ends up finding generalizing solutions.

A tractable way to study GD’s implicit regularization is to focus on properties shared by solutions that GD dynamics can practically reach and maintain. This viewpoint is strongly motivated by the empirical “Edge of Stability” (EoS) phenomenon, where training with large learning rates operates near a critical stability boundary determined by a balance between step size and local loss curvature (Cohen et al., 2020). It is also supported by theoretical analyses of discrete-time GD stability (Wu et al., 2018; Nar & Sastry, 2018; Mulayoff et al., 2021; Nacson et al., 2023; Damian et al., 2024), which make precise that stability imposes a sharpness/curvature constraint that is intrinsic to the dynamics. Motivated by these works, we study the stability-constrained region as a proxy for GD’s implicit regularization. The guiding problem is then to understand how much effective capacity remains after imposing this stability constraint.

Recent work provides a coherent answer for two-layer ReLU fully connected networks (FCNs). In FCNs, the stability

constraint induces data-dependent regularity controls and the strength of this regularity is governed by the ambient input data geometry (Liang et al., 2026; 2025; Qiao et al., 2024; Mulayoff et al., 2021; Nacson et al., 2023). In particular, Liang et al. (2026; 2025) show that as the input distribution concentrates closer to a sphere, stability-based guarantees can deteriorate, and in the extreme hyperspherical setting the stability constraint yields no generalization guarantee for FCNs.

However, this prediction does not align cleanly with modern computer vision practice. Standard normalization preprocessing often maps images close to a hypersphere, precisely the geometry where FCN-based BEoS guarantees are weakest (Liang et al., 2026). Yet, CNNs trained on such normalized data can still generalize well. This discrepancy suggests that ambient geometry and GD stability alone do not tell the whole story. A missing ingredient is architectural inductive bias, which changes the way the model processes the input. In a CNN, the model applies the same filter to many local patches of the image and then aggregates the resulting responses. This viewpoint motivates an explicit “patch” formulation: we represent an input as a collection of patches, apply a shared computation to each patch, and then aggregate. Consequently, the gradient of a shared filter is an aggregate of its patch-wise gradients, rather than a gradient computed from the whole image viewed as one vector.

We capture exactly these ingredients with a minimal two-layer locally connected ReLU network with weight sharing (LCN-WS), where fixed coordinate projections extract patches and a single set of hidden weights is shared across spatial locations. With this patch notation, a two-layer convolutional layer with shared filters is a special case of LCN-WS, and the gradient with respect to the shared weights coincides with the gradient of the corresponding CNN parameters. This abstraction keeps locality and weight sharing while remaining tractable for stability-based analysis.

Contributions. In this paper, motivated by empirical Edge-of-Stability behavior in CNN training, we develop a stability-based theory for locally connected networks with weight sharing (LCN-WS) and use it to connect *architecture* (locality and weight sharing), *data geometry* (the prior of the patch point cloud), and *implicit regularization* under large-step-size GD.

1. We show that in LCN-WS, a stability constraint implies an explicit regularity control in terms of a weighted path norm whose weights are governed by the geometry of the induced patch multiset. This extends stability-induced complexity controls for FCNs (Liang et al., 2025; Qiao et al., 2024) and makes precise that convolutional patch extraction transfers the relevant data dependence from ambient inputs to the *distribution of*

local patches.

2. Leveraging this characterization, we prove that when the receptive field size is small relative to ambient dimension ($m \ll d$), the BEoS class of LCN-WS admits nontrivial generalization guarantees on hyperspherical data. In contrast, under the same ambient geometry, FCNs can have vacuous BEoS-based guarantees (Liang et al., 2026). In particular, in the regime of fixed m and large d , our bounds yield a polynomial-rate upper bound on the generalization gap of the form $n^{-\frac{1}{\delta} + O(\frac{m}{d})}$ up to log factors (see Theorem 4.2). The theoretical results are numerically supported by synthetic experiments that probe the scaling of the generalization gap with n and d . This separation demonstrates that architectural inductive bias can cooperate with stability constraints by changing the representation geometry that stability “sees”.
3. We give a flat interpolation construction showing that, without distributional assumptions, there exist datasets where an LCN-WS can interpolate while still satisfying the BEoS condition (Theorem 4.3). This clarifies why additional data priors are necessary for stability-induced generalization.
4. We provide empirical evidence that natural-image patches extracted by standard convolutional receptive fields exhibit a patch geometry that is compatible with strong BEoS-induced implicit regularization in Section 5.1. We also introduce a clustered-patch synthetic model to isolate the role of weight sharing by contrasting FCN, LCN (no sharing), and LCN-WS, and we demonstrate that sharing couples filters to the global patch distribution in a manner consistent with our stability-based mechanism in Section 5.2.

From this perspective, we summarize that the *inductive bias of CNNs comes from the distributional structure of local image patches induced by convolutional receptive fields and natural-image priors, and this structure makes GD gravitate toward generalizable features*.

2. Related Work

Patch-based representation learning. Early unsupervised image representation methods decomposed images into local patches and learned sparse dictionaries or manifolds from these primitives. K-SVD represented images as sparse linear combinations of learned dictionary elements (Aharon et al., 2006), and natural image patches were shown to lie near low-dimensional manifolds of patch spaces (Peyré, 2009). Patch based representations have also shown success in unsupervised learning (Paulin et al., 2017), as we as using unsupervised embeddings as a preprocessing to learning

image classifiers (Coates et al., 2011; Thiry et al., 2021; Brutzkus et al., 2022). These results highlight that patch space is highly structured, but how neural network training exploits such structure remains open; our work helps bridge this gap through a dynamical stability analysis of GD.

Geometric awareness in training neural networks Recent theoretical work has explored how architectural design incorporates geometric awareness to improve neural network training and approximation. Approximation theory research (Mhaskar et al., 2017; Zhou, 2020; Poggio, 2022; Poggio & Fraser, 2024) demonstrates that CNN architectures overcome the curse of dimensionality inherent in the pixel space by exploiting compositional structure in natural images. This advantage is formalized by (Mao et al., 2021), which establishes the theoretical superiority of CNNs over fully connected networks (FCNs) for learning certain composite functions. However, these results differ from ours as our work generalizes to the overparameterized regime. More recently, Vision Transformers (ViTs) (Dosovitskiy, 2020) have emerged as a leading architecture for visual tasks, and explicitly tokenizes patches of an image. Shi et al. (2025) extends the approximation-theoretic results to ViTs, showing that they outperform FCNs in approximation rates for compositional functions. Additional work has identified patch extraction, rather than the attention mechanism, as the critical component enabling ViTs to generate effective features (Trockman & Kolter, 2022), further reinforcing the strength of locally connected architectures. Alternatively, our results do not require any assumptions on the label function satisfying a compositional (or any) structure.

Theoretical analysis of CNNs. CNNs and ResNets have been theoretically studied (Oono & Suzuki, 2019; Liu et al., 2021; Zhang et al., 2024) from the approximation-theoretic angles. It was established that CNNs with appropriate level of sparse weights can estimate functions large function classes with near-minimax optimal sample complexity (Oono & Suzuki, 2019) and adapt to the intrinsic dimensions when the data are supported on a low-dimensional manifold (Liu et al., 2021). Zhang et al. (2024) further established the same results in overparameterized regimes under weight decay. However, these results rely on reducing CNNs to the standard approximation-theory of fully connected neural networks (Yarotsky, 2017), thus do not reveal the same architectural insights specific to CNNs as we described in this paper. Specifically, we do not require the input data to be supported on a low-dimensional manifold to avoid the curse-of-dimensionality. We also do not require explicit regularization such as weight decay or a sparsity constraint.

Separation of CNNs from FCNs The statistical separation of CNNs and FCNs has been established (Li et al., 2021; Wang & Wu, 2023; Lahoti et al., 2024). This line of work inspected the sample complexity of CNN models in learning

certain regression functions, and established a hierarchy of sample complexity of $\Theta(\log^2(d))$, $\Theta(d)$, $\Theta(d^2)$ for CNN, CNN without weight sharing (LCNs) and FCNs respectively. Our results are for the same models (CNNs with and without weight sharing) family, but different in that we considered an overparameterized regime without explicit regularization. Interestingly, the more realistic setting allows us to prove an exponentially stronger separation between FCNs and LCNs (and CNNs). Lastly, the significance of the input data distribution (rather than the labeling functions) was not discovered in prior work.

Implicit regularization of gradient descent. Many existing work on the implicit bias of gradient descent relies on strong assumptions on the data distributions (e.g., linear separable data), simplified model architectures (e.g., linear activation) to make a gradient dynamics analysis tractable (Soudry et al., 2018; Gunasekar et al., 2018a;b), or weight initialization schemes that keep the model in the kernel regimes (Jacot et al., 2018; Arora et al., 2019). While CNNs were studied (Gunasekar et al., 2018b; Arora et al., 2019), the nature of the results are different from ours.

Edge of stability, minima stability, and generalization by large stepsizes. Our approach builds upon a recent line of work that studies the set of solutions that gradient descent can visit (or converge to) via either Edge-of-stability observation or the minima stability theory (Ding et al., 2024; Mulayoff et al., 2021; Nacson et al., 2023; Qiao et al., 2024; Liang et al., 2025; 2026). These approaches enable formal analysis of the generalization properties without having to analyze gradient dynamics. To the best of our knowledge, they all focused on feedforward neural networks, and we are the first to study CNNs and the impact of model architecture choices in the implicit bias of large stepsizes.

3. Preliminaries and Notations

Throughout the paper, we use $O(\cdot)$, $\Omega(\cdot)$ to absorb constants while $\tilde{O}(\cdot)$ absorb logarithmic factors. \mathbb{S}^{d-1} means the unit hypersphere in \mathbb{R}^d and \mathbb{B}_R^d means a d -dimensional ball of radius R . Moreover, we set $[n] = \{1, 2, \dots, n\}$.

Architectures. Fix integers $d \geq 1$ and $1 \leq m \leq d$. A local receptive field of size m is a coordinate subset $S_j \subset [d]$ and induces coordinate projections $\pi_j: \mathbb{R}^d \rightarrow \mathbb{R}^m$ by selecting coordinates in S_j . We denote $\mathbf{x}^{(S_j)} := \pi_j(\mathbf{x})$ and call it a (generalized) patch. One may regard π_j as a patch extractor, $\pi_j(\mathbf{x})$ as a patch and the space \mathbb{R}^m as the patch space.

We consider two-layer locally connected networks with weight sharing. To instantiate such a model, we need to specify a set of local receptive fields $\mathcal{S} = \{S_j\}_{j=1}^J$. Given such \mathcal{S} and a width $K \in \mathbb{N}$, a two-layer \mathcal{S} -connected ReLU network with weight sharing and Global Average Pooling

(GAP) is implemented by

$$f_{\boldsymbol{\theta}}(\mathbf{x}) = \sum_{k=1}^K v_k \left(\frac{1}{J} \sum_{j=1}^J \phi(\mathbf{w}_k^{\top} \pi_j(\mathbf{x}) - b_k) \right) + \beta \quad (1)$$

The parameters $\boldsymbol{\theta} = \{(v_k, \mathbf{w}_k, b_k)\}_{k=1}^K \cup \{\beta\}$ are in $\mathbb{R}^{(m+2)K+1}$, and *weight sharing* means that the same filters $\{(\mathbf{w}_k, b_k)\}_{k=1}^K$ are used across all $j \in [J]$. Let Θ_K^S denote the parameter set for width K , and $\Theta^S := \bigcup_{K \geq 1} \Theta_K^S$. We assume $\mathbf{w}_k \neq \mathbf{0}$ for all k , otherwise the corresponding neuron can be absorbed into β . A unit of $\phi(\mathbf{w}_k^{\top} \cdot - b_k)$ in the network is called a *filter* or a *neuron*.

Data and loss function. A dataset is $\mathcal{D} = \{(\mathbf{x}_i, y_i)\}_{i=1}^n \subset \mathbb{B}_R^d \times [-D, D]$. We use the squared loss and define the empirical objective $\mathcal{L}(\boldsymbol{\theta}) := \frac{1}{2n} \sum_{i=1}^n (f_{\boldsymbol{\theta}}(\mathbf{x}_i) - y_i)^2$.

“Edge of Stability” regime. Empirical and theoretical work (Cohen et al., 2020; Damian et al., 2024) suggests that GD with large learning rate often reaches a regime where the linear stability threshold governs the sharpness: along the GD trajectory, there is typically a “progressive sharpening” phase in which $\lambda_{\max}(\nabla^2 \mathcal{L}(\boldsymbol{\theta}_t))$ increases, until it approaches the “Edge of Stability” scale $2/\eta$, where η is the learning rate. Throughout this paper, GD refers to vanilla GD with learning rate η and we assume $\eta < 2$.

Definition 3.1 (Below Edge of Stability (BEoS) (Qiao et al., 2024, Definition 2.3)). Let $\{\boldsymbol{\theta}_t\}_{t \geq 1}$ be the GD trajectory on \mathcal{L} with learning rate η . We say the trajectory is *Below-Edge-of-Stability (BEoS)* if there exists $t^* > 0$ such that for all $t \geq t^*$,

$$\lambda_{\max}(\nabla^2 \mathcal{L}(\boldsymbol{\theta}_t)) \leq \frac{2}{\eta}.$$

Any parameter state $\boldsymbol{\theta}_t$ with $t \geq t^*$ is referred to as a *BEoS solution*.

This condition applies to any twice-differentiable solution produced by GD, even when GD does not converge.

For our analysis it is convenient to study the set of *all* parameters that satisfies the BEoS condition

$$\Theta_{\text{BEoS}}^S(\eta, \mathcal{D}) := \left\{ \boldsymbol{\theta} \in \Theta^S \mid \lambda_{\max}(\nabla^2 \mathcal{L}(\boldsymbol{\theta})) \leq \frac{2}{\eta} \right\}. \quad (2)$$

Statistical learning and generalization gap. For the data generalization process, we assume the data points $\{(\mathbf{x}_i, y_i)\}_{i=1}^n$ are i.i.d. sampled from a distribution \mathcal{P} defined on $\mathbb{B}_R^d \times [-D, D]$. The “test-time performance” of a predictor f on unseen data is accounted by the *population risk* $R(f) := \mathbb{E}_{(\mathbf{x}, y) \sim \mathcal{P}} [(f(\mathbf{x}) - y)^2]$ (in this paper we consider the MSE loss for regression tasks). The training time performance on \mathcal{D} is accounted by the empirical risk $\widehat{R}_{\mathcal{D}}(f) = \frac{1}{n} \sum_{i=1}^n (f(\mathbf{x}_i) - y_i)^2$. The generalization gap

is defined to be the absolute difference between empirical risk and population risk $\text{GeneralizationGap}(f, \mathcal{D}) := |R(f) - \widehat{R}_{\mathcal{D}}(f)|$, which is abbreviated by $\text{Gen}_{\mathcal{D}}(f)$.

The non-parametric regression with noisy labels on the random design is one typical setting in this program. Suppose $\{\mathbf{x}_i\}_{i=1}^n$ are i.i.d. sampled from a distribution $\mathcal{P}_{\mathbf{X}}$ supported on \mathbb{B}_R^d and $y_i = f_{\text{true}}(\mathbf{x}_i) + \xi_i$ for $i \in [n]$, where $f_{\text{true}}: \mathbb{R}^d \rightarrow \mathbb{R}$ is the ground-true function and $\{\xi_i\}_{i=1}^n$ are i.i.d. Gaussian noises $\mathcal{N}(0, \sigma^2)$. In this setting, the goal of the regression task is to find a predictor f to minimize the mean squared error (MSE):

$$\text{MSE}(f) = \frac{1}{n} \sum_{i=1}^n (f(\mathbf{x}_i) - f_{\text{true}}(\mathbf{x}_i))^2. \quad (3)$$

The population level of (3) is known as *excess risk*,

$$\text{Excess}(f) := \mathbb{E}_{\mathbf{x} \sim \mathcal{P}_{\mathbf{X}}} [(f(\mathbf{x}) - f_{\text{true}}(\mathbf{x}))^2], \quad (4)$$

which is also called the *estimation error* under $L^2(\mathcal{P}_{\mathbf{X}})$.

In this setting, the population risk (under squared loss) of a predictor f decomposes as

$$R(f) = \mathbb{E}_{(\mathbf{x}, y) \sim \mathcal{P}} [(f(\mathbf{x}) - y)^2] = \text{Excess}(f) + \sigma^2, \quad (5)$$

The additive term σ^2 is the irreducible error contributed by the label noise, and it is achieved by the Bayes predictor $f^*(\mathbf{x}) = \mathbb{E}[y \mid \mathbf{x}] = f_{\text{true}}(\mathbf{x})$, namely $R(f^*) = \sigma^2$. Consequently, $R(f) - R(f^*) = \mathbb{E}_{\mathbf{x} \sim \mathcal{P}_{\mathbf{X}}} [(f(\mathbf{x}) - f_{\text{true}}(\mathbf{x}))^2]$, so controlling the excess risk is equivalent to controlling the population regret in squared-loss regression.

Moreover, the generalization gap in this random-design regression model admits the following equivalent form

$$\text{Gen}(f, \mathcal{D}) = \left| \text{Excess}(f) + \sigma^2 - \widehat{R}_{\mathcal{D}}(f) \right|. \quad (6)$$

This identity makes explicit how the generalization gap compares the *population* performance (excess risk plus irreducible noise) against the *training* performance measured by the empirical squared loss.

4. Main Results.

This section characterizes the implicit regularization below the edge of stability for locally connected networks with weight sharing (LCN-WS), and derives a generalization guarantee under spherical inputs.

We first show that every predictor $f_{\boldsymbol{\theta}}$ with $\boldsymbol{\theta} \in \Theta_{\text{BEoS}}^S(\eta, \mathcal{D})$ satisfies an explicit regularity control in the form of a weighted path norm. The weight function depends on the empirical patch geometry induced by the receptive fields \mathcal{S} , and it quantifies the stability cost of placing a hidden unit at a given activation boundary in patch space.

Given a dataset $\mathcal{D} = \{(\mathbf{x}_i, y_i)\}_{i=1}^n$ and receptive fields $\mathcal{S} = \{S_j\}_{j=1}^J$, let $\mathbf{X}_{\mathcal{D}}^S$ be a random vector drawn uniformly from the $\{\pi_j(\mathbf{x}_i)\}_{(i,j) \in [n] \times [J]} \subset \mathbb{R}^m$. We consider an associated patch-space weight function $g_{\mathcal{D},S}: \mathbb{S}^{m-1} \times \mathbb{R} \rightarrow \mathbb{R}$, where $\mathbb{S}^{m-1} := \{\mathbf{u} \in \mathbb{R}^m \mid \|\mathbf{u}\|_2 = 1\}$ denotes the unit sphere. The weight function is defined by $g_{\mathcal{D},S}(\mathbf{u}, t) := \min\{\tilde{g}_{\mathcal{D},S}(\mathbf{u}, t), \tilde{g}_{\mathcal{D},S}(-\mathbf{u}, -t)\}$, where

$$\tilde{g}_{\mathcal{D},S}(\mathbf{u}, t) := \mathbb{P}(\mathbf{u}^\top \mathbf{X}_{\mathcal{D}}^S > t)^2 \mathbb{E}[\mathbf{u}^\top \mathbf{X}_{\mathcal{D}}^S - t \mid \mathbf{u}^\top \mathbf{X}_{\mathcal{D}}^S > t] \times \sqrt{1 + \left\| \mathbb{E}[\mathbf{X}_{\mathcal{D}}^S \mid \mathbf{u}^\top \mathbf{X}_{\mathcal{D}}^S > t] \right\|_2^2}. \quad (7)$$

We now state the stability-to-regularity implication.

Theorem 4.1. Fix $\mathcal{D} = \{(\mathbf{x}_i, y_i)\}_{i=1}^n$ and local receptive fields \mathcal{S} . For any $\boldsymbol{\theta} \in \Theta_K^S$ in the model (1),

$$\sum_{k=1}^K |v_k| \|\mathbf{w}_k\| g_{\mathcal{D},S} \left(\frac{\mathbf{w}_k}{\|\mathbf{w}_k\|}, \frac{b_k}{\|\mathbf{w}_k\|} \right) \leq \frac{1}{2} \left(\lambda_{\max}(\nabla^2 \mathcal{L}(\boldsymbol{\theta})) + 2(R+1)\sqrt{2\mathcal{L}(\boldsymbol{\theta})} - 1 \right). \quad (8)$$

Specifically, for any $\boldsymbol{\theta} \in \Theta_{\text{BEoS}}^S(\eta, \mathcal{D})$, we have

$$\sum_{k=1}^K |v_k| \|\mathbf{w}_k\| g_{\mathcal{D},S} \left(\frac{\mathbf{w}_k}{\|\mathbf{w}_k\|}, \frac{b_k}{\|\mathbf{w}_k\|} \right) \leq \frac{1}{\eta} - \frac{1}{2} + (R+1)\sqrt{2\mathcal{L}(\boldsymbol{\theta})}. \quad (9)$$

The detailed proof is deferred to Appendix B. Equation (9) shows that BEoS controls a weighted path norm, where each neuron is penalized according to the activation mass of its patch-space hyperplane. The factor $\mathbb{P}(\mathbf{u}^\top \mathbf{X}_{\mathcal{D}}^S > t)^2$ in (7) is the main activation-mass term: if a neuron is active on few patches, then this probability is small, which makes $\tilde{g}_{\mathcal{D},S}(\mathbf{u}, t)$ small and weakens the stability penalty on that neuron. Intuitively, $g_{\mathcal{D},S}$ penalizes neurons that are active on a large fraction of patches, as they contribute significantly to the Hessian. A detailed derivation connecting the Hessian contribution of a patch-space hyperplane to (7) is given in Proposition B.9.

When $m = d$ (and implicitly $J = 1$), Theorem 4.1 reduces to the fully connected case, recovering the stability-to-regularity results in (Liang et al., 2025), see also (Qiao et al., 2024; Nacson et al., 2023). In this setting, $g_{\mathcal{D},S}$ becomes an ambient-space weight $g_{\mathcal{D}}$. For spherical data, (Liang et al., 2025) constructs interpolating fully connected networks by placing activation boundaries that isolate individual data points in the ambient space, which forces $\mathbb{P}(\mathbf{u}^\top \mathbf{X}_{\mathcal{D}} > t)$ and hence $g_{\mathcal{D}}(\mathbf{u}, t)$ to be arbitrarily small as n grows. The LCN-WS setting differs only in where this geometry is evaluated: (\mathbf{u}, t) now describes a hyperplane in patch space, and weight sharing ties the same hyperplane across all receptive fields.

4.1. Generalization analysis for LCN-WS on spherical data

We specialize to the setting where the marginal input distribution is $\text{Uniform}(\mathbb{S}^{d-1})$ and derive a stability-based upper bound on the generalization gap implied by the regularity control in Theorem 4.1. In particular, in the regime where m is fixed and $d \rightarrow \infty$, the resulting rate scales as $n^{-\frac{1}{6} + O(m/d)}$ (up to logarithmic factors). Thus, there is no curse of dimensionality, and the bound can even improve with d (a ‘‘blessing of dimensionality’’). By contrast, in the same setting FCNs admit no non-trivial generalization upper bound (see Liang et al., 2026).

Theorem 4.2. Suppose \mathcal{P} is a joint distribution of (\mathbf{x}, y) . Assume that the marginal distribution of \mathbf{x} is $\text{Uniform}(\mathbb{S}^{d-1})$ and the marginal distribution of y is supported on $[-D, D]$ for some $D > 0$. Fix a dataset $\mathcal{D} = \{(\mathbf{x}_i, y_i)\}_{i=1}^n$, where each data point is drawn i.i.d. from \mathcal{P} . Let $M \geq D$. Assume $d > 3$ and $1 \leq m < \frac{d(d-3)}{d+3}$, if $\boldsymbol{\theta} \in \Theta_{\text{BEoS}}^S(\eta, \mathcal{D})$ and $\|f_{\boldsymbol{\theta}}\|_{\infty} \leq M$, then, with probability $\geq 1 - 2\delta$, we have that for the plug-in risk estimator $\widehat{R}_{\mathcal{D}}(f) := \frac{1}{n} \sum_{i=1}^n (f(\mathbf{x}_i) - y_i)^2$,

$$\left| \mathbb{E}_{(\mathbf{x}, y) \sim \mathcal{P}} \left[(f_{\boldsymbol{\theta}}(\mathbf{x}) - y)^2 \right] - \widehat{R}_{\mathcal{D}}(f_{\boldsymbol{\theta}}) \right| \lesssim_d \text{poly}(d, A, J, M) n^{-\frac{(d-m)(d+3)}{2(3d^2 - md + 3d - 3m)}}, \quad (10)$$

Here $A = \frac{1}{\eta} - 1 + 4M$, and \lesssim_d hides constants depending only on d and logarithmic factors in n and (J/δ) .

In particular, if m is fixed and $d \rightarrow \infty$, the leading-order behavior is $A^{\frac{1}{3}} J^{\frac{1}{3}} M^{\frac{11}{6}} n^{-\frac{1}{6}}$ (up to log factors).

The full proof appears in Appendix C. Here we provide a high-level intuition for why generalization become *better* as the ambient dimension d grows (a ‘‘blessing of dimensionality’’).

When $m \ll d$ and \mathbf{x} is roughly isotropic on \mathbb{S}^{d-1} , most of the signal energy is dispersed across many coordinates. As a result, the m -dimensional patch projections $\pi_j(\mathbf{x}) \in \mathbb{R}^m$ typically have small norm, meaning that (in patch space) most patches concentrate near the origin rather than lying near the boundary.

This concentration has two consequences for implicit regularization. First, many patches of a typical input look ‘‘similar’’ in magnitude, so when a filter becomes active on one patch, it tends to be compatible with (and hence effectively couples to) a large fraction of the other patches as well. Second, this coupling makes the architecture-induced weight function g comparatively large on the bulk of the data distribution, which amplifies the stability-driven control captured by our theory.

In short, increasing d while keeping patch size m fixed

makes it increasingly unlikely that any single patch dominates the norm, so typical inputs are governed by many small, well-behaved patches; weight sharing then propagates constraints across those patches, yielding a stronger effective regularity and improved generalization.

4.1.1. NUMERICAL VALIDATIONS

We use synthetic data to empirically validate our claims that LCN-WS generalizes well on spherical data when $m \ll d$, and the rate does not deteriorate as the ambient dimension increases. We adopt the random-design non-parametric regression setting introduced in Section 3.

Fix a collection of receptive fields $\mathcal{S} = \{S_j\}_{j=1}^J$ with patch size m . In all experiments we use disjoint coordinate patches $S_j = \{(j-1)m+1, \dots, jm\}$ so that $J = \lfloor d/m \rfloor$. We first sample a ground-truth predictor $f_{true} \in \Theta^{\mathcal{S}}$ from the LCN architecture in (1) with a moderate width $K_{true} = 20$ (fixed across all n), and generate training inputs $\{\mathbf{x}_i\}_{i=1}^n$ i.i.d. from $\text{Uniform}(\mathbb{S}^{d-1})$. The labels are generated by $y_i = f_{true}(\mathbf{x}_i) + \xi_i$, where $\xi_i \sim \mathcal{N}(0, \sigma^2)$ are i.i.d Gaussian noise. We also generate an independent test set $\{\tilde{\mathbf{x}}_r\}_{r=1}^N \sim \text{Uniform}(\mathbb{S}^{d-1})$ (with $N \gg n$) for Monte Carlo evaluation of the excess risk.

We compare two overparameterized two-layer ReLU models trained by full-batch GD: (i) **LCN-WS** (two layer \mathcal{S} -connected ReLU network with weight sharing in (1)), and (ii) **FCN** obtained by taking $m = d$ and $J = 1$ in (1).

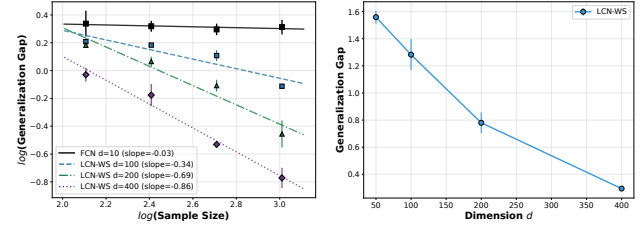
Unless otherwise stated, both models use width $K = 1024$, which places the training in an overparameterized regime for the sample sizes we consider.

For each trained predictor f , we report (i) **train loss** $\widehat{R}_{\mathcal{D}}(f)$ This quantity measures how well the predictor fit the training set; (ii) **estimated population excess risk** (cf. (4)) $\widehat{\text{Excess}}(f) := \frac{1}{N} \sum_{r=1}^N (f(\tilde{\mathbf{x}}_r) - f_{true}(\tilde{\mathbf{x}}_r))^2$, via an independent test set, which measures how well the predictor matches the ground truth; (iii) **estimated generalization gap**, $\widehat{\text{Gen}}(f, \mathcal{D}) := |\widehat{\text{Excess}}(f) + \sigma^2 - \widehat{R}_{\mathcal{D}}(f)|$, which is aligned with (6) and is the main object predicted by our theory (Theorem 4.2).

To estimate the sample-size scaling, we sweep $n \in \{128, 256, 512, 1024\}$ and repeat the full pipeline over multiple random seeds. We plot $\log \widehat{\text{Gen}}(f_{\hat{\theta}}, \mathcal{D})$ versus $\log n$ and report the least-squares fitted slope (**LCN-WS**: $d = 100, 200, 400$; **FCN**: $d = 10$).

4.2. When will LCN-WS stably overfit?

Theorem 4.2 relies on paying an explicit probability term for inputs whose induced patches lie near the boundary of \mathbb{B}_1^m . This is necessary and the following worst-case construction shows that without controlling the contribution



(a) Log–log scaling with n .

(b) Gap versus d (fixed n).

Figure 2. Generalization-gap scaling in synthetic experiments. (Left) $\widehat{\text{Gen}}(f_{\hat{\theta}}, \mathcal{D})$ versus the sample size n on a log–log scale. The fitted slope summarizes the empirical rate: if $\text{GenGap} \lesssim n^{-c}$, then $\log(\text{GenGap}) \leq -c \log n + b$, so a more negative slope indicates faster decay (better generalization). In our experiments, the FCN slope is nearly flat (slope = -0.03 at $d = 10$), whereas LCN-WS exhibits increasingly negative slopes as d grows (slope = -0.34 at $d = 100$, -0.69 at $d = 200$, and -0.86 at $d = 400$), indicating faster decay with n . (Right) $\widehat{\text{Gen}}(f_{\hat{\theta}}, \mathcal{D})$ versus the ambient dimension d with n fixed, illustrating that for LCN-WS (with patch size $m \ll d$) the generalization gap remains stable and can even decrease as d increases.

of such inputs, BEoS constraint alone cannot guarantee generalization once the patch multiset “tricking” the flatness criterion to allow interpolating LCN-WS.

Theorem 4.3 (Stable interpolation with width $\leq n$). *Assume that all the patches $\{\pi_j(\mathbf{x}_i)\}$ are on \mathbb{S}^{m-1} . There exists a width $K \leq n$ network of the form (1) that interpolates the dataset and whose Hessian operator norm satisfies*

$$\lambda_{\max}(\nabla_{\theta}^2 \mathcal{L}) \leq 1 + \frac{D^2 + 2/J^2}{n}. \quad (11)$$

In particular, if we remove the output bias parameter β , then $\lambda_{\max}(\nabla_{\theta}^2 \mathcal{L}) \leq \frac{D^2 + 2/J^2}{n}$.

The constructive proof is presented in Appendix D. Intuitively, the assumption in Theorem 4.3 provides, for each labeled example, a unit-norm patch \mathbf{p}_i that is unique among all patches in the dataset, such that one can construct a hidden unit whose patch-space activation boundary activates on \mathbf{p}_i and is inactive on all other patches, and use $K \leq n$ such units to interpolate. Since each unit is active on essentially one patch in the patch multiset, the activation-mass term $\mathbb{P}(\mathbf{u}^{\top} \mathbf{X}_{\mathcal{D}}^{\mathcal{S}} > t)$ of each “memorizing” neuron is small and the corresponding stability cost in (9) is weak.

The result that BEoS does not provide a distribution-free capacity control for LCN-WS. More specifically, if one consider the non-parametric estimation setting as we introduced in the Section 3 with noise level $\sigma^2 > 0$, then for any interpolation solution $f_{\hat{\theta}}$, namely $\mathcal{L}(\hat{\theta}) = 0$, the generalization gap is at least σ^2 according to (6).

Remark 4.4. Increasing evidence shows that ReLU neural networks do not benignly overfit (Mallinar et al., 2022; Haas et al., 2023). Therefore, the existence of these interpolating

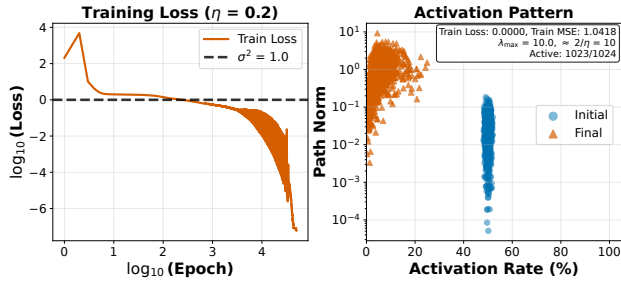


Figure 3. Stable interpolation may still happen. An LCN-WS trained with $\eta = 0.2$ interpolates noisy labels while stable $\lambda_{\max} \approx \frac{2}{\eta} = 10$. **(Right)** The concentration of neurons of low-rate activation indicates that the stable interpolating network exploits the property exhibited by $\mathcal{G}_{D,S}$.

LCN-WS should demonstrate the BEoS constraint cannot generalize in the worst case.

5. Patch Geometry as a Data Prior for Convolutional Inductive Bias

Theorem 4.3 shows that, without distributional assumptions, architectural locality and weight sharing together with the BEoS proxy do not yield a meaningful capacity control: if the empirical patch multiset admits patch-level isolation, then there exist stably interpolating LCN-WS solutions. This motivates a practice-facing question. Under standard convolutional local receptive fields, what patch geometry do real-world images induce, and how does gradient descent under large step sizes interact with this geometry?

5.1. The geometry of natural-image patches

In this subsection we analyze CIFAR-10. We extract standard 3×3 convolutional receptive fields (stride 1, padding 0), sample 10^7 patches from the training set, and use the standard torchvision normalization. Intuitively, the resulting patch cloud is much more “structured” than the cloud of whole images: most variability is captured by a few dominant directions, and it is harder for a single hyperplane to carve out a tiny subset of patches (i.e., typical cuts do not nearly isolate individual points). To quantify this, Figure 4 compares the induced patch cloud with the ambient image cloud.

To quantify this effect, we adopt the data-geometry framework of (Liang et al., 2026) based on half-space depth. We start by recalling the notion of *half-space depth* (a.k.a. *Tukey depth*). Let \mathcal{P} be a distribution on \mathbb{R}^m and let $\mathbf{X} \sim \mathcal{P}$. For a point $z \in \mathbb{R}^m$, its half-space depth is $\text{depth}(z; \mathcal{P}) := \inf_{\mathbf{u} \in \mathbb{S}^{m-1}} \mathbb{P}(\mathbf{u}^\top \mathbf{X} \geq \mathbf{u}^\top z)$. Equivalently, $\text{depth}(z; \mathcal{P})$ is the smallest probability mass of a (closed) half-space that contains z . Thus, larger depth means z is more “central” in the distribution, while small

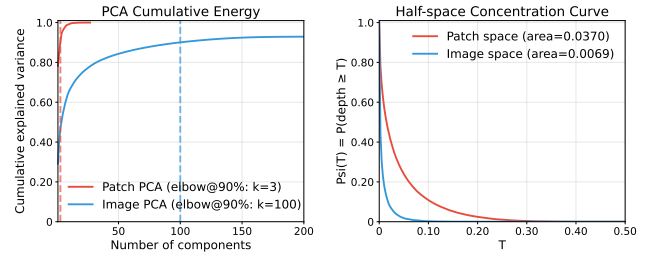


Figure 4. Patch geometry vs. image geometry on CIFAR-10. The patch point cloud is significantly of lower intrinsic dimension. **(Left)**: PCA explained-variance curves for the patch cloud (dimension $m = 27$, but 3 directions dominates 90% variance) and the ambient image cloud (dimension $d = 3072$, and need more than 100 directions to dominate 90% variance). **(Right)**: half-space concentration curves $\Psi(T)$; larger area indicates more deep points and fewer opportunities for near-isolating ReLU hyperplanes.

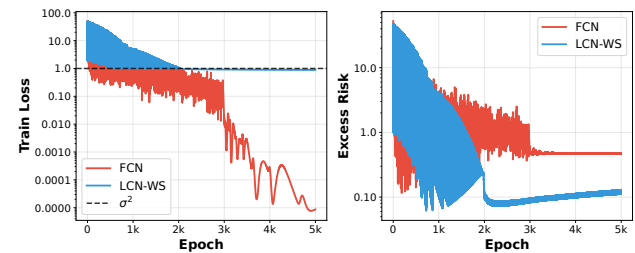


Figure 5. Real-data validation on CIFAR-10. We compare FCN and LCN-WS on a nonparametric regression task with noisy labels, using inputs sampled from CIFAR-10. Here LCN-WS denotes a CNN with a 3×3 kernel (stride 1, no padding). **(Left)** FCN memorizes noise (train loss $\ll \sigma^2$), whereas LCN-WS plateaus near the noise floor. **(Right)** LCN-WS achieves decreasing excess risk while FCN fails to learn. This behavior is consistent with Figure 4: the patch point cloud appears more structured than the full image cloud, which can induce stronger implicit regularization.

depth indicates that there exists a hyperplane through z that leaves only a small fraction of points on one side.

The distribution of depths is captured by the concentration curve $\Psi_{\mathcal{P}}(T) := \mathbb{P}(\text{depth}(\mathbf{X}; \mathcal{P}) \geq T)$ for $T \in [0, 1/2]$. A larger area under $\Psi_{\mathcal{P}}$ indicates that typical points have larger depth.

We apply this setup to the empirical patch distribution induced by convolutional receptive fields. We report the PCA explained-variance curves and the half-space concentration curves for both patches and images in Figure 4.

5.2. Learning the cluster of patches: the role of weight sharing

Beyond the low-dimensionality and low-shatterability, Brutzkus et al. (2022) demonstrate that natural-image patches exhibit cluster structure: k -means on CIFAR-10/ImageNet patches achieves small centroid distances once $k \geq 50$, with most patches forming uninformative

background clusters while few concentrate around label-informative patterns. In this subsection, we investigate whether the stability regularization helps GD learn informative clusters in the patch space. In particular, we simulate this “patch-cluster feature learning” phenomenon in a minimal synthetic distribution, and use it as an ablation to isolate the role of *weight sharing* in driving the feature-learning behavior predicted by our stability analysis.

Data generation process. We construct inputs by partitioning $\mathbf{x} \in \mathbb{R}^D$ into J disjoint patches $\mathbf{x}^{(1)}, \dots, \mathbf{x}^{(J)} \in \mathbb{R}^m$ with $D = Jm$. The patch multiset contains one dominant *noise cluster* and two small *signal clusters*. Concretely, fix two unit vectors $\mathbf{v}_+, \mathbf{v}_- \in \mathbb{S}^{m-1}$. For each sample, draw a label $y \in \{\mathbf{v}_+, \mathbf{v}_-\}$ uniformly and choose a signal location $j^* \sim \text{Uniform}([J])$. Set the signal patch to be a noisy version of the label, $\mathbf{x}^{(j^*)} = \mathbf{y} + \xi_{j^*}$, while all other patches are pure noise, $\mathbf{x}^{(j)} = \xi_j$ for $j \neq j^*$, with $\xi_j \sim \mathcal{N}(0, \sigma^2 \mathbf{I})$. We choose σ so that the total noise energy is fixed (independent of J, m). The learning problem is a regression problem.

This distribution captures two properties that are typical in vision: (i) *sparse feature in space* only one patch per image carries label-relevant signal; and (ii) *clustered patch geometry*: most patches lie near the noise cluster, while the rare informative patches lie near the two signal centers $\{\mathbf{v}_+, \mathbf{v}_-\}$. We compare three overparameterized two-layer ReLU models trained with the same optimizer and step size: FCN, LCN (without sharing), and LCN-WS.

The weight-sharing ablation Fig 6 confirms this mechanism is specific to LCN-WS. Without sharing, each location can fit idiosyncratic patch subsets more easily, weakening the coupling between a single filter and the *global* patch distribution that drives the activation-mass penalty. This makes patch-level isolation strategies more accessible and reduces the effectiveness of stability-induced regularity as a guardrail against memorization. The toy model thus provides a controlled demonstration that sharing (together with pooling) is a key ingredient behind the generalization advantage of CNN-style architectures.

6. Discussion of Limitations and Future Work

We revisit our paradigm from the perspective of gradient dynamics.

In the setting of this paper, consider the patch matrix $\mathbf{X} \in \mathbb{R}^{(nJ) \times m}$ whose row indexed by (i, j) equals $\pi_j(\mathbf{x}_i)^\top$. Define the lifted residual vector $\bar{\mathbf{r}} \in \mathbb{R}^{nJ}$ by $(\bar{\mathbf{r}})_{(i,j)} := r_i$. Let $\mathbf{S}(\boldsymbol{\theta}) \in \{0, 1\}^{(nJ) \times K}$ be the gating matrix

$$\mathbf{S}(\boldsymbol{\theta})_{(i,j),k} := \mathbb{1}\{\mathbf{w}_k^\top \pi_j(\mathbf{x}_i) > b_k\},$$

and let $\mathbf{v} := (v_1, \dots, v_K)^\top$. Stack first-layer weights as $\mathbf{W} := [\mathbf{w}_1^\top; \dots; \mathbf{w}_K^\top] \in \mathbb{R}^{K \times m}$. A direct calculation gives a backprop-aligned factorization of the gradient. Define the

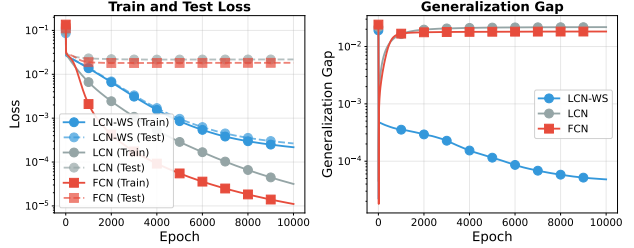


Figure 6. Weight sharing enables generalization Train (solid) and test (dashed) loss on the clustered-patch distribution. All architectures fit the training data but only LCN-WS generalizes. LCN without weight sharing fails like FCN, demonstrating that locality alone is insufficient—weight sharing couples filters to global patch geometry, enabling stronger stability-induced regularity.

patch-level backprop signal

$$\mathbf{R}(\boldsymbol{\theta}) := \frac{1}{nJ} \bar{\mathbf{r}} \mathbf{v}^\top \in \mathbb{R}^{(nJ) \times K}, \quad \mathbf{G}(\boldsymbol{\theta}) := \mathbf{R}(\boldsymbol{\theta}) \odot \mathbf{S}(\boldsymbol{\theta}),$$

where \odot denotes entrywise multiplication. Then we have

$$\nabla_{\mathbf{W}} \mathcal{L}(\boldsymbol{\theta}) = \mathbf{G}(\boldsymbol{\theta})^\top \mathbf{X}. \quad (12)$$

The matrix $\mathbf{G}(\boldsymbol{\theta})$ aggregates the learning signal generated by the residuals, the linear readout weights, and the gates. The matrix \mathbf{X} then maps this signal into parameter updates. In this sense, \mathbf{X} acts as a “signal rectifier”: data priors and architecture jointly shape the geometry of \mathbf{X} , thereby governing the effective directions along which the gradient dynamics can move. For example, Figure 4 shows that, for CIFAR-10, 90% of the energy of the convolutional patch matrix is concentrated in three principal directions, suggesting a strong geometric constraint on the gradient dynamics.

At the same time, a direct dynamical analysis becomes intractable in the *overparameterized feature-learning regime*. For this reason, we use stability as a proxy for implicit regularization. The terms appearing in the definition of $g_{\mathcal{D},S}$ are drawn from the same ingredients as (12), e.g. the gate statistics induced by $\mathbf{S}(\boldsymbol{\theta})$ and the geometry encoded by \mathbf{X} . Accordingly, the stability proxy is well suited to characterize where the dynamics *cannot go* (implicit regularization), but it is less informative about which stable solution the dynamics *prefer* (implicit bias). A more detailed dynamical account of the implicit bias is left for future work.

Although our analysis focuses on shallow networks, the underlying viewpoint may also inform the study of feature learning in deep neural networks. During backpropagation, if we fix a particular layer, then \mathbf{X} in (12) should be interpreted as the hidden representation matrix produced by the preceding layers. In particular, for an attention block in a ViT, a natural question is: as the training set scales, what representation geometry does attention induce that allows its generalization performance to remain competitive with CNNs? We also left this question in future investigation.

Impact Statement

This paper presents theoretical work aimed at advancing our understanding of why convolutional neural networks generalize. We analyze how architectural choices—locality and weight sharing—interact with optimization dynamics to induce implicit regularization. This work does not introduce new systems or applications with direct societal consequences. We hope that improved theoretical understanding of neural network generalization will contribute to more novel and principled architecture designs

References

- NIST digital library of mathematical functions. <http://dlmf.nist.gov/>. See §5.6(i), Eq. 5.6.E4 for Gautschi’s inequality (Gamma ratio bounds).
- Aharon, M., Elad, M., and Bruckstein, A. K-svd: An algorithm for designing overcomplete dictionaries for sparse representation. *IEEE Transactions on signal processing*, 54(11):4311–4322, 2006.
- Arora, S., Du, S. S., Hu, W., Li, Z., Salakhutdinov, R. R., and Wang, R. On exact computation with an infinitely wide neural net. *Advances in neural information processing systems*, 32, 2019.
- Arpit, D., Jastrzebski, S., Ballas, N., Krueger, D., Bengio, E., Kanwal, M. S., Maharaj, T., Fischer, A., Courville, A. C., Bengio, Y., and Lacoste-Julien, S. A closer look at memorization in deep networks. In *Proceedings of the 34th International Conference on Machine Learning (ICML)*, pp. 233–242. PMLR, 2017.
- Brutzkus, A., Globerson, A., Malach, E., Netser, A. R., and Shalev-Schwartz, S. Efficient learning of cnns using patch based features. In *International Conference on Machine Learning*, pp. 2336–2356. PMLR, 2022.
- Coates, A., Ng, A., and Lee, H. An analysis of single-layer networks in unsupervised feature learning. In *Proceedings of the fourteenth international conference on artificial intelligence and statistics*, pp. 215–223. JMLR Workshop and Conference Proceedings, 2011.
- Cohen, J., Kaur, S., Li, Y., Kolter, J. Z., and Talwalkar, A. Gradient descent on neural networks typically occurs at the edge of stability. In *International Conference on Learning Representations*, 2020.
- Damian, A., Nichani, E., and Lee, J. D. Self-stabilization: The implicit bias of gradient descent at the edge of stability. In *International Conference on Learning Representations*, 2024.
- Ding, L., Drusvyatskiy, D., Fazel, M., and Harchaoui, Z. Flat minima generalize for low-rank matrix recovery. *Information and Inference: A Journal of the IMA*, 13(2):iaae009, 2024.
- Dosovitskiy, A. An image is worth 16x16 words: Transformers for image recognition at scale. *arXiv preprint arXiv:2010.11929*, 2020.
- Fukushima, K. Neocognitron: A hierarchical neural network capable of visual pattern recognition. *Neural networks*, 1(2):119–130, 1988.
- Gunasekar, S., Lee, J., Soudry, D., and Srebro, N. Characterizing implicit bias in terms of optimization geometry. In *International Conference on Machine Learning*, pp. 1832–1841. PMLR, 2018a.
- Gunasekar, S., Lee, J. D., Soudry, D., and Srebro, N. Implicit bias of gradient descent on linear convolutional networks. *Advances in neural information processing systems*, 31, 2018b.
- Haas, M., Holzmüller, D., Luxburg, U., and Steinwart, I. Mind the spikes: Benign overfitting of kernels and neural networks in fixed dimension. *Advances in Neural Information Processing Systems*, 36, 2023.
- Haussler, D. Decision-theoretic generalizations of the pac model for neural net and other learning applications. *Information and Computation*, 100(1):78–150, 1992.
- He, K., Zhang, X., Ren, S., and Sun, J. Deep residual learning for image recognition. In *Proceedings of the IEEE conference on computer vision and pattern recognition*, pp. 770–778, 2016.
- Jacot, A., Gabriel, F., and Hongler, C. Neural tangent kernel: Convergence and generalization in neural networks. *Advances in neural information processing systems*, 31, 2018.
- Krizhevsky, A., Sutskever, I., and Hinton, G. E. Imagenet classification with deep convolutional neural networks. *Advances in neural information processing systems*, 25, 2012.
- Lahoti, A., Karp, S., Winston, E., Singh, A., and Li, Y. Role of locality and weight sharing in image-based tasks: A sample complexity separation between cnns, lcns, and fcns. In *The Twelfth International Conference on Learning Representations*, 2024.
- Lai, C.-H., Song, Y., Kim, D., Mitsufuji, Y., and Ermon, S. The principles of diffusion models. *arXiv preprint arXiv:2510.21890*, 2025.

- LeCun, Y., Bottou, L., Bengio, Y., and Haffner, P. Gradient-based learning applied to document recognition. *Proceedings of the IEEE*, 86(11):2278–2324, 2002.
- Li, Z., Zhang, Y., and Arora, S. Why are convolutional nets more sample-efficient than fully-connected nets? In *International Conference on Learning Representations*, 2021.
- Liang, T., Qiao, D., Wang, Y.-X., and Parhi, R. Stable minima of ReLU neural networks suffer from the curse of dimensionality: The neural shattering phenomenon. In *Advances in Neural Information Processing Systems (NeurIPS)*, 2025.
- Liang, T., Cloninger, A., Parhi, R., and Wang, Y.-X. Generalization below the edge of stability: The role of data geometry. In *International Conference on Learning Representations (ICLR)*, 2026.
- Liu, H., Chen, M., Zhao, T., and Liao, W. Besov function approximation and binary classification on low-dimensional manifolds using convolutional residual networks. In *International Conference on Machine Learning*, pp. 6770–6780. PMLR, 2021.
- Mallinar, N., Simon, J., Abedsoltan, A., Pandit, P., Belkin, M., and Nakkiran, P. Benign, tempered, or catastrophic: Toward a refined taxonomy of overfitting. *Advances in Neural Information Processing Systems*, 35:1182–1195, 2022.
- Mao, T., Shi, Z., and Zhou, D.-X. Theory of deep convolutional neural networks iii: Approximating radial functions. *Neural Networks*, 144:778–790, 2021.
- Mhaskar, H., Liao, Q., and Poggio, T. When and why are deep networks better than shallow ones? In *Proceedings of the AAAI conference on artificial intelligence*, volume 31, 2017.
- Mohri, M., Rostamizadeh, A., and Talwalkar, A. *Foundations of Machine Learning*. MIT Press, second edition, 2018.
- Mulayoff, R., Michaeli, T., and Soudry, D. The implicit bias of minima stability: A view from function space. *Advances in Neural Information Processing Systems*, 34:17749–17761, 2021.
- Nacson, M. S., Mulayoff, R., Ongie, G., Michaeli, T., and Soudry, D. The implicit bias of minima stability in multivariate shallow ReLU networks. In *International Conference on Learning Representations*, 2023.
- Nar, K. and Sastry, S. Step size matters in deep learning. *Advances in Neural Information Processing Systems*, 31, 2018.
- Oono, K. and Suzuki, T. Approximation and non-parametric estimation of resnet-type convolutional neural networks. In *International conference on machine learning*, pp. 4922–4931. PMLR, 2019.
- Parhi, R. and Nowak, R. D. Near-minimax optimal estimation with shallow ReLU neural networks. *IEEE Transactions on Information Theory*, 69(2):1125–1139, 2023.
- Paulin, M., Mairal, J., Douze, M., Harchaoui, Z., Perronnin, F., and Schmid, C. Convolutional patch representations for image retrieval: an unsupervised approach. *International Journal of Computer Vision*, 121(1):149–168, 2017.
- Peyré, G. Manifold models for signals and images. *Computer vision and image understanding*, 113(2):249–260, 2009.
- Poggio, T. Foundations of deep learning: Compositional sparsity of computable functions. Technical report, CBMM memo 138, 2022.
- Poggio, T. and Fraser, M. Compositional sparsity of learnable functions. *Bulletin of the American Mathematical Society*, 61(3):438–456, 2024.
- Qiao, D., Zhang, K., Singh, E., Soudry, D., and Wang, Y.-X. Stable minima cannot overfit in univariate ReLU networks: Generalization by large step sizes. In *Advances in Neural Information Processing Systems*, volume 37, pp. 94163–94208, 2024.
- Ronneberger, O., Fischer, P., and Brox, T. U-net: Convolutional networks for biomedical image segmentation. In *International Conference on Medical image computing and computer-assisted intervention*, pp. 234–241. Springer, 2015.
- Shi, Z., Fang, Z., and Cao, Y. Approximation and estimation capability of vision transformers for hierarchical compositional models. *Applied and Computational Harmonic Analysis*, pp. 101849, 2025.
- Siegel, J. W. and Xu, J. Characterization of the variation spaces corresponding to shallow neural networks. *Constructive Approximation*, pp. 1–24, 2023.
- Soudry, D., Hoffer, E., Nacson, M. S., Gunasekar, S., and Srebro, N. The implicit bias of gradient descent on separable data. *Journal of Machine Learning Research*, 19(70):1–57, 2018.
- Thiry, L., Arbel, M., Belilovsky, E., and Oyallon, E. The unreasonable effectiveness of patches in deep convolutional kernels methods. *arXiv preprint arXiv:2101.07528*, 2021.

- Trockman, A. and Kolter, J. Z. Patches are all you need? *arXiv preprint arXiv:2201.09792*, 2022.
- Wainwright, M. J. *High-dimensional statistics: A non-asymptotic viewpoint*, volume 48. Cambridge university press, 2019.
- Wang, Z. and Wu, L. Theoretical analysis of the inductive biases in deep convolutional networks. *Advances in Neural Information Processing Systems*, 36:74289–74338, 2023.
- Wu, L., Ma, C., and E, W. How SGD selects the global minima in over-parameterized learning: A dynamical stability perspective. *Advances in Neural Information Processing Systems*, 31, 2018.
- Yarotsky, D. Error bounds for approximations with deep relu networks. *Neural networks*, 94:103–114, 2017.
- Zhang, C., Bengio, S., Hardt, M., Recht, B., and Vinyals, O. Understanding deep learning requires rethinking generalization. In *International Conference on Learning Representations (ICLR)*, 2017. URL <https://openreview.net/forum?id=Sy8gdB9xx>.
- Zhang, Z., Zhang, K., Chen, M., Takeda, Y., Wang, M., Zhao, T., and Wang, Y.-X. Nonparametric classification on low dimensional manifolds using overparameterized convolutional residual networks. *Advances in Neural Information Processing Systems*, 37:65738–65764, 2024.
- Zhou, D.-X. Universality of deep convolutional neural networks. *Applied and computational harmonic analysis*, 48 (2):787–794, 2020.

A. Functional Analysis of Shallow ReLU Networks

A.1. Path-norm and Variation Semi-norm of ReLU Networks

This subsection collects several basic facts from (Parhi & Nowak, 2023) and (Siegel & Xu, 2023) that we will use later.

Definition A.1. Let $f_\theta(\mathbf{x}) = \sum_{k=1}^K v_k \phi(\mathbf{w}_k^\top \mathbf{x} - b_k) + \beta$ be a fully-connected two-layer neural network. The (unweighted) path-norm of f_θ is defined to be

$$\|f_\theta\|_{\text{path}} := \sum_{k=1}^K |v_k| \|\mathbf{w}_k\|_2. \quad (13)$$

Dictionary representation of ReLU networks. Using the positive 1-homogeneity of ReLU, one may rescale each hidden unit while leaving the realized function unchanged:

$$v_k \phi(\mathbf{w}_k^\top \mathbf{x} - b_k) = a_k \phi(\mathbf{u}_k^\top \mathbf{x} - t_k), \quad \mathbf{u}_k := \frac{\mathbf{w}_k}{\|\mathbf{w}_k\|_2} \in \mathbb{S}^{d-1}, \quad t_k := \frac{b_k}{\|\mathbf{w}_k\|_2}, \quad a_k := v_k \|\mathbf{w}_k\|_2.$$

Consequently, f_θ can be written in the normalized finite-sum form

$$f(\mathbf{x}) = \sum_{k=1}^{K'} a_k \phi(\mathbf{u}_k^\top \mathbf{x} - t_k) + \mathbf{c}^\top \mathbf{x} + c_0. \quad (14)$$

Define the (ReLU) ridge dictionary as $\mathcal{D}_\phi := \{\phi(\mathbf{u}^\top \cdot -t) : \mathbf{u} \in \mathbb{S}^{d-1}, t \in \mathbb{R}\}$. We focus on the *overparameterized, width-agnostic* collection obtained by taking the *union over all finite widths*

$$\mathcal{F}_{\text{fin}} := \bigcup_{K \geq 1} \left\{ \sum_{k=1}^K a_k \phi(\mathbf{u}_k^\top \cdot -t_k) + \mathbf{c}^\top (\cdot) + c_0 \right\}, \quad (15)$$

and quantify complexity via the smallest path-norm among all realizations of f :

$$\|f\|_{\text{path}, \min} := \inf \{ \|f_\theta\|_{\text{path}} : f_\theta \equiv f \text{ of the form (14)} \}.$$

From finite sums to a width-agnostic integral representation. Rather than fixing a particular width K , it is convenient to work with a convex, measure-theoretic formulation that *captures the closure/convex hull of (15)*. Concretely, let ν be a finite signed Radon measure on $\mathbb{S}^{d-1} \times [-R, R]$ and consider

$$f(\mathbf{x}) = \int_{\mathbb{S}^{d-1} \times [-R, R]} \phi(\mathbf{u}^\top \mathbf{x} - t) d\nu(\mathbf{u}, t) + \mathbf{c}^\top \mathbf{x} + c_0. \quad (16)$$

Every finite network of the form (14) corresponds to an *atomic* (hence sparse) measure $\nu = \sum_{k=1}^K a_k \delta_{(\mathbf{u}_k, t_k)}$, and conversely any such atomic ν yields a finite network. Therefore, (16) should be viewed as a *width-agnostic relaxation* aligned with (13), rather than as an assumption of an infinite-width limit.

Definition A.2. The (unweighted) variation (semi)norm

$$|f|_{\mathcal{V}} := \inf \{ \|\nu\|_{\mathcal{M}} : f \text{ admits (14) for some } (\nu, \mathbf{c}, c_0) \}, \quad (17)$$

where $\|\nu\|_{\mathcal{M}}$ is the total variation of ν .

For the compact region $\Omega = \mathbb{B}_R^d$, we define the bounded variation function class as

$$\mathcal{V}_C(\Omega) := \left\{ f : \Omega \rightarrow \mathbb{R} \mid f = \int_{\mathbb{S}^{d-1} \times [-R, R]} \phi(\mathbf{u}^\top \mathbf{x} - t) d\nu(\mathbf{u}, t) + \mathbf{c}^\top \mathbf{x} + b, |f|_{\mathcal{V}} \leq C \right\}. \quad (18)$$

In particular, identifying (14) with the atomic measure $\nu = \sum_k a_k \delta_{(\mathbf{u}_k, t_k)}$ yields

$$|f|_{\mathbb{V}} \leq \sum_k |a_k| = \|f_{\theta}\|_{\text{path}}, \quad \text{hence} \quad |f|_{\mathbb{V}} \leq \|f\|_{\text{path}, \min}.$$

Moreover, the minimal total variation required to represent f coincides with the minimal path-norm over all finite decompositions:

$$\|f\|_{\text{path}, \min} = |f|_{\mathbb{V}}. \quad (19)$$

Thus, (17) provides a *nonparametric* analogue of the path-norm: it encodes the same complexity notion while *not committing to a fixed width* K .

Remark A.3 (“Arbitrary width” \neq “infinite width”). All statements here are about \mathcal{F}_{fin} in (15), namely networks of *finite* (but unconstrained) width. The integral representation (16) is introduced as a convenient convexification/closure of this union for analysis and regularization; it *does not* posit an infinite-width limit. In particular, when training in the variational form with a total-variation penalty on ν , first-order optimality implies that optimal measures are sparse (i.e., have finite support), which corresponds exactly to *finite-width* networks. Therefore, our results hold for *arbitrary (yet finite) width*; the continuum measure serves only as a tool to characterize and control $\|f\|_{\text{path}, \min}$.

A.2. The Metric Entropy of Variation Spaces

Metric entropy is a standard way to describe how “compact” a subset A is inside a metric space (X, ρ_X) . We recall the notions of covering numbers and metric entropy.

Definition A.4 (Covering Number and Entropy). Let A be a compact subset of a metric space (X, ρ_X) . For $t > 0$, the *covering number* $N(A, t, \rho_X)$ is the smallest number of closed balls of radius t whose union contains A :

$$N(t, A, \rho_X) := \min \left\{ N \in \mathbb{N} : \exists x_1, \dots, x_N \in X \text{ s.t. } A \subset \bigcup_{i=1}^N \mathbb{B}(x_i, t) \right\}, \quad (20)$$

where $\mathbb{B}(x_i, t) = \{y \in X : \rho_X(y, x_i) \leq t\}$. The *metric entropy* of A at scale t is then

$$H_t(A)_X := \log N(t, A, \rho_X). \quad (21)$$

Covering/entropy bounds for bounded-variation-type classes have been established in the literature. In what follows, we will use the estimate stated below.

Proposition A.5 (Parhi & Nowak 2023, Appendix D). *The metric entropy of $V_C(\mathbb{B}_R^d)$ (see Definition A.2) with respect to the $L^\infty(\mathbb{B}_R^d)$ -distance $\|\cdot\|_\infty$ satisfies*

$$\log N(t, V_C(\mathbb{B}_R^d), \|\cdot\|_\infty) \lesssim_d \left(\frac{C}{t}\right)^{\frac{2d}{d+3}}. \quad (22)$$

where \lesssim_d hides constants (which could depend on d) and logarithmic factors.

A.3. Generalization Gap of Unweighted Variation Function Class

As a middle step towards bounding the generalization gap of the weighted variation function class, we bound the generalization gap of the unweighted variation function class using chaining and Gaussian complexity, together with the L^∞ metric entropy bound in Proposition A.5.

Proposition A.6 (Wainwright 2019, Chapter 13). *Fix design points $\mathbf{x}_1, \dots, \mathbf{x}_n$ and denote the empirical norm*

$$\|f\|_n^2 := \frac{1}{n} \sum_{i=1}^n f(\mathbf{x}_i)^2.$$

Let \mathcal{F} be a class of real-valued functions on $\{\mathbf{x}_i\}_{i=1}^n$, and define

$$\widehat{\mathcal{G}}_n(\mathcal{F}) := \sup_{f \in \mathcal{F}} \frac{1}{n} \sum_{i=1}^n \varepsilon_i f(\mathbf{x}_i), \quad \varepsilon_1, \dots, \varepsilon_n \stackrel{i.i.d.}{\sim} \mathcal{N}(0, 1), \quad \mathcal{G}_n(\mathcal{F}) := \mathbb{E} \widehat{\mathcal{G}}_n(\mathcal{F}).$$

Then

$$\mathcal{G}_n(\mathcal{F}) \lesssim \frac{16}{\sqrt{n}} \int_0^{\text{diam}(\mathcal{F}, \|\cdot\|_n)} \sqrt{\log N(t, \mathcal{F}, \|\cdot\|_n)} dt, \quad (23)$$

where $\text{diam}(\mathcal{F}, \|\cdot\|_n) := \sup_{f_1, f_2 \in \mathcal{F}} \|f_1 - f_2\|_n$. Moreover, with probability at least $1 - \delta$,

$$\widehat{\mathcal{G}}_n(\mathcal{F}) \leq \mathcal{G}_n(\mathcal{F}) + \text{diam}(\mathcal{F}, \|\cdot\|_n) \frac{\sqrt{\log(1/\delta)}}{\sqrt{n}} \quad (\delta > 0). \quad (24)$$

Lemma A.7. Let $\mathcal{F}_{M,C} = \{f \in V_C(\mathbb{B}_R^d) \mid \|f\|_\infty \leq M\}$ with $M \geq D$, and let $\mathcal{D} = \{(\mathbf{x}_i, y_i)\}_{i=1}^n \sim \mathcal{P}^{\otimes n}$ where $|Y| \leq D$ a.s. Then with probability at least $1 - \delta$,

$$\sup_{f \in \mathcal{F}_{M,C}} |R(f) - \widehat{R}_{\mathcal{D}}(f)| \lesssim_d C^{\frac{d}{d+3}} M^{\frac{d+6}{d+3}} n^{-\frac{1}{2}} + M^2 \left(\frac{\log(1/\delta)}{n} \right)^{\frac{1}{2}}. \quad (25)$$

Proof. Let $\ell_f(\mathbf{x}, y) := (y - f(\mathbf{x}))^2$ and $\mathcal{L}_{M,C} := \{\ell_f : f \in \mathcal{F}_{M,C}\}$. Since $|y| \leq D \leq M$ and $\|f\|_\infty \leq M$, for any $f, g \in \mathcal{F}_{M,C}$ and any (\mathbf{x}, y) ,

$$|\ell_f(\mathbf{x}, y) - \ell_g(\mathbf{x}, y)| = |f(\mathbf{x}) - g(\mathbf{x})| |f(\mathbf{x}) + g(\mathbf{x}) - 2y| \leq 4M |f(\mathbf{x}) - g(\mathbf{x})|.$$

Therefore, for the empirical norm on $\{\mathbf{x}_i\}_{i=1}^n$,

$$\|\ell_f - \ell_g\|_n \leq 4M \|f - g\|_n \leq 4M \|f - g\|_\infty, \quad (26)$$

and $\text{diam}(\mathcal{L}_{M,C}, \|\cdot\|_n) \leq 8M^2$.

A standard Gaussian symmetrization/concentration argument (see, e.g., [Wainwright 2019](#), Chapter 5) yields that with probability at least $1 - \delta$,

$$\sup_{f \in \mathcal{F}_{M,C}} |R(f) - \widehat{R}_{\mathcal{D}}(f)| \lesssim \widehat{\mathcal{G}}_n(\mathcal{L}_{M,C}) + M^2 \left(\frac{\log(1/\delta)}{n} \right)^{\frac{1}{2}}. \quad (27)$$

It remains to bound $\widehat{\mathcal{G}}_n(\mathcal{L}_{M,C})$ by chaining. By (26), any t -cover of $\mathcal{F}_{M,C}$ in $\|\cdot\|_n$ induces a $(4Mt)$ -cover of $\mathcal{L}_{M,C}$ in $\|\cdot\|_n$, hence

$$\log N(t, \mathcal{L}_{M,C}, \|\cdot\|_n) \leq \log N\left(\frac{t}{4M}, \mathcal{F}_{M,C}, \|\cdot\|_n\right) \leq \log N\left(\frac{t}{4M}, V_C(\mathbb{B}_R^d), \|\cdot\|_\infty\right),$$

where we used $\|h\|_n \leq \|h\|_\infty$. Proposition A.5 then gives, up to logarithmic factors,

$$\log N(t, \mathcal{L}_{M,C}, \|\cdot\|_n) \lesssim_d \left(\frac{MC}{t} \right)^{\frac{2d}{d+3}}.$$

Applying Proposition A.6 with $\mathcal{G} = \mathcal{L}_{M,C}$ and $\text{diam}(\mathcal{L}_{M,C}, \|\cdot\|_n) \leq 8M^2$ yields

$$\begin{aligned} \widehat{\mathcal{G}}_n(\mathcal{L}_{M,C}) &\lesssim_d \frac{1}{\sqrt{n}} \int_0^{8M^2} \left(\frac{MC}{t} \right)^{\frac{d}{d+3}} dt + M^2 \left(\frac{\log(1/\delta)}{n} \right)^{\frac{1}{2}} \\ &\lesssim_d C^{\frac{d}{d+3}} M^{\frac{d+6}{d+3}} n^{-\frac{1}{2}} + M^2 \left(\frac{\log(1/\delta)}{n} \right)^{\frac{1}{2}}. \end{aligned}$$

Combining with (27) proves (25). \square

B. Proof of Theorem 4.1

Let $\iota_j : \mathbb{R}^m \rightarrow \mathbb{R}^d$ be the dual embedding such that $\pi_j \circ \iota_j = \text{id}_{\mathbb{R}^m}$. Then (1) is equivalent to a fully connected neural network in a form of

$$f_{\theta}(\mathbf{x}) = \sum_{k=1}^K \frac{1}{J} \sum_{j=1}^J v_k \phi(\iota_j(\mathbf{w}_k)^{\top} \mathbf{x} - b_k) + \beta. \quad (28)$$

Note that for any fixed k , $\|\iota_j(\mathbf{w}_k)\|_2 = \|\mathbf{w}_k\|_2$ for all $j = 1, \dots, J$. Therefore, the notion of path norm and variation norm (together with their weighted version) still make sense for the CNN model

$$\|f_{\theta}\|_{\text{path}} = \frac{1}{J} \sum_{k=1}^K \sum_{j=1}^J |v_k| \|\iota_j(\mathbf{w}_k)\|_2 = \sum_{k=1}^K |v_k| \|\mathbf{w}_k\|_2. \quad (29)$$

By direct computation, the Hessian matrix of the loss function is expressed as

$$\nabla_{\theta}^2 \mathcal{L} = \underbrace{\frac{1}{n} \sum_{i=1}^n \nabla_{\theta} f(\mathbf{x}_i) \nabla_{\theta} f(\mathbf{x}_i)^{\top}}_{\mathbf{T}_{\mathcal{D}}} + \underbrace{\frac{1}{n} \sum_{i=1}^n (f(\mathbf{x}_i) - y_i) \nabla_{\theta}^2 f(\mathbf{x}_i)}_{\mathbf{R}_{\mathcal{D}}}. \quad (30)$$

Definition B.1. Given a dataset $\mathcal{D} = \{(\mathbf{x}_i, y_i)\}_{i=1}^n$ and a set of local receptive fields $\mathcal{S} = \{S_j\}_{j=1}^J$, we define a random vector $\mathbf{X}_{\mathcal{D}}^{\mathcal{S}}$ uniformly draw from $\{\pi_j(\mathbf{x}_i)\}_{(i,j)}^{n \times J} \subset \mathbb{R}^m$. For any $\mathbf{u} \in \mathbb{S}^{m-1}$, $t \in \mathbb{R}$, we define the weight function

$$g_{\mathcal{D}, \mathcal{S}}(\mathbf{u}, t) = \min \left\{ \tilde{g}_{\mathcal{D}, \mathcal{S}}(\mathbf{u}, t), \tilde{g}_{\mathcal{D}, \mathcal{S}}(-\mathbf{u}, -t) \right\}. \quad (31)$$

where

$$\tilde{g}_{\mathcal{D}, \mathcal{S}}(\mathbf{u}, t) := \mathbb{E} \left[\phi(\mathbf{u}^{\top} \mathbf{X}_{\mathcal{D}}^{\mathcal{S}} - t) \right] \sqrt{\mathbb{P}(\mathbf{u}^{\top} \mathbf{X}_{\mathcal{D}}^{\mathcal{S}} > t)^2 + \left\| \mathbb{E} \left[\mathbf{X}_{\mathcal{D}}^{\mathcal{S}} \mathbb{1}\{\mathbf{u}^{\top} \mathbf{X}_{\mathcal{D}}^{\mathcal{S}} > t\} \right] \right\|_2^2}. \quad (32)$$

Note that (32) is equivalent to (7).

Proposition B.2. Given a data set $\mathcal{D} = \{\mathbf{x}_i, y_i\}_{i=1}^n$ and a network model (1) with local receptive fields \mathcal{S} . Then we have

$$\lambda_{\max}(\mathbf{T}_{\mathcal{D}}) \geq 1 + 2 \sum_{k=1}^K |v_k| \|\mathbf{w}_k\| g_{\mathcal{D}, \mathcal{S}} \left(\frac{\mathbf{w}_k}{\|\mathbf{w}_k\|}, \frac{b_k}{\|\mathbf{w}_k\|} \right). \quad (33)$$

Proof. We write $\mathbf{T}_{\mathcal{D}}$ in terms of tangent features

$$\mathbf{T}_{\mathcal{D}} = \frac{1}{n} \sum_{i=1}^n \nabla_{\theta} f(\mathbf{x}_i) \nabla_{\theta} f(\mathbf{x}_i)^{\top} = \frac{1}{n} \Phi \Phi^{\top}.$$

Consequently,

$$\lambda_{\max}(\mathbf{T}_{\mathcal{D}}) = \max_{\mathbf{u} \in \mathbb{S}^{n-1}} \frac{1}{n} \|\Phi \mathbf{u}\|^2 \geq \frac{1}{n^2} \|\Phi \mathbf{1}\|^2. \quad (34)$$

For any point \mathbf{x} and abbreviate its patch extraction on S_j by $\mathbf{x}^{(S_j)} := \pi_j(\mathbf{x})$. Define the ReLU gate

$$m_k^{(S_j)}(\mathbf{x}) := \mathbb{1} \left\{ \mathbf{w}_k^{\top} \mathbf{x}^{(S_j)} > b_k \right\}.$$

For any sample \mathbf{x}_i , denote $m_{k,i}^{(S_j)} := m_k^{(S_j)}(\mathbf{x}_i)$. Then the partial derivatives are

$$\frac{\partial f(\mathbf{x}_i)}{\partial v_k} = \frac{1}{J} \sum_{j=1}^J m_{k,i}^{(S_j)} \cdot (\mathbf{w}_k^{\top} \mathbf{x}_i^{(S_j)} - b_k), \quad \frac{\partial f(\mathbf{x}_i)}{\partial \mathbf{w}_k} = \frac{1}{J} \sum_{j=1}^J m_{k,i}^{(S_j)} \cdot v_k \cdot \mathbf{x}_i^{(S_j)},$$

$$\frac{\partial f(\mathbf{x}_i)}{\partial b_k} = -\frac{1}{J} \sum_{j=1}^J m_{k,i}^{(S_j)} \cdot v_k, \quad \frac{\partial f(\mathbf{x}_i)}{\partial \beta} = 1.$$

Stacking these over i and plugging $u = \mathbf{1}/\sqrt{n}$ in (34), we get

$$\begin{aligned} \frac{1}{n^2} \|\Phi \mathbf{1}\|^2 &= 1 + \frac{1}{n^2} \sum_{k=1}^K \left[(v_k)^2 \left(\left\| \sum_{i=1}^n \frac{1}{J} \sum_{j=1}^J m_{k,i}^{(S_j)} \mathbf{x}_i^{(S_j)} \right\|^2 + \left(\sum_{i=1}^n \frac{1}{J} \sum_{j=1}^J m_{k,i}^{(S_j)} \right)^2 \right) \right. \\ &\quad \left. + \left(\sum_{i=1}^n \frac{1}{J} \sum_{j=1}^J \phi(\mathbf{w}_k^\top \mathbf{x}_i^{(S_j)} - b_k) \right)^2 \right] \\ &= 1 + \frac{1}{n^2} \sum_{k=1}^K \left[(v_k)^2 \left(\left\| \sum_{i=1}^n \frac{1}{J} \sum_{j=1}^J m_{k,i}^{(S_j)} \mathbf{x}_i^{(S_j)} \right\|^2 + \left(\sum_{i=1}^n \frac{1}{J} \sum_{j=1}^J m_{k,i}^{(S_j)} \right)^2 \right) \right. \\ &\quad \left. + \|\mathbf{w}_k\|_2^2 \left(\sum_{i=1}^n \frac{1}{J} \sum_{j=1}^J \phi(\mathbf{u}_k^\top \mathbf{x}_i^{(S_j)} - t_k) \right)^2 \right] \tag{35} \\ &\geq 1 + \frac{2}{n^2} \sum_{k=1}^K |v_k| \|\mathbf{w}_k\|_2 \left(\sum_{i=1}^n \frac{1}{J} \sum_{j=1}^J \phi(\mathbf{u}_k^\top \mathbf{x}_i^{(S_j)} - t_k) \right) \\ &\quad \cdot \sqrt{\left\| \sum_{i=1}^n \frac{1}{J} \sum_{j=1}^J m_{k,i}^{(S_j)} \mathbf{x}_i^{(S_j)} \right\|^2 + \left(\sum_{i=1}^n \frac{1}{J} \sum_{j=1}^J m_{k,i}^{(S_j)} \right)^2} \quad (\text{since } a^2 + b^2 \geq 2ab) \\ &= 1 + 2 \sum_{k=1}^K |v_k| \|\mathbf{w}_k\|_2 \left(\frac{1}{nJ} \sum_{i=1}^n \sum_{j=1}^J \phi(\mathbf{u}_k^\top \mathbf{x}_i^{(S_j)} - t_k) \right) \\ &\quad \cdot \sqrt{\left\| \frac{1}{nJ} \sum_{i=1}^n \sum_{j=1}^J m_{k,i}^{(S_j)} \mathbf{x}_i^{(S_j)} \right\|^2 + \left(\frac{1}{nJ} \sum_{i=1}^n \sum_{j=1}^J m_{k,i}^{(S_j)} \right)^2} \\ &= 1 + 2 \sum_{k=1}^K |v_k| \|\mathbf{w}_k\|_2 \mathbb{E} [\phi(\mathbf{u}^\top \mathbf{X}_D^S - t)] \sqrt{\mathbb{P}(\mathbf{u}^\top \mathbf{X}_D^S > t)^2 + \left\| \mathbb{E}[\mathbf{X}_D^S \mathbf{1}\{\mathbf{u}^\top \mathbf{X}_D^S > t\}] \right\|^2} \\ &= 1 + 2 \sum_{k=1}^K |v_k| \|\mathbf{w}_k\|_2 \tilde{g}_{\mathcal{D},S}(\mathbf{u}_k, t_k), \quad \mathbf{u}_k = \frac{\mathbf{w}_k}{\|\mathbf{w}_k\|_2}, \quad t_k = \frac{b_k}{\|\mathbf{w}_k\|_2}. \end{aligned}$$

Then combining (34) and the above inequality yields the claim (and replacing \tilde{g} by $g = \min\{\tilde{g}(\mathbf{u}, t), \tilde{g}(-\mathbf{u}, -t)\}$ keeps a valid lower bound). \square

Lemma B.3. Consider the model (1)

$$f(\mathbf{x}) = \sum_{k=1}^K \frac{v_k}{J} \sum_{j=1}^J \phi(\mathbf{w}_k^\top \pi_j(\mathbf{x}) - b_k) + \beta.$$

where the input satisfies $\|\mathbf{x}\|_2 \leq R$, each patch extractor $\pi_j : \mathbb{R}^d \rightarrow \mathbb{R}^m$ is a coordinate projection, and $\phi(t) = \max\{0, t\}$. Let $\boldsymbol{\theta} = (\mathbf{w}_1^\top, \dots, \mathbf{w}_K^\top, b_1, \dots, b_K, v_1, \dots, v_K, \beta)^\top$ collect all parameters. Assume $f_{\boldsymbol{\theta}}(\mathbf{x})$ is twice differentiable with respect to $\boldsymbol{\theta}$ at \mathbf{x} , i.e., for all k and $S_j \in \mathcal{S}$ we have $\mathbf{w}_k^\top \mathbf{x}^{(S_j)} \neq b_k$. Then for any perturbation vector $\boldsymbol{\omega}$ with $\|\boldsymbol{\omega}\|_2 = 1$, it holds that

$$|\boldsymbol{\omega}^\top \nabla_{\boldsymbol{\theta}}^2 f_{\boldsymbol{\theta}}(\mathbf{x}) \boldsymbol{\omega}| \leq 2(R+1).$$

Proof. Write $\boldsymbol{\theta} = (\mathbf{w}_1^\top, \dots, \mathbf{w}_K^\top, b_1, \dots, b_K, v_1, \dots, v_K, \beta)^\top$. The total number of parameters is $N = K \cdot m + K + K + 1 = K(m + 2) + 1$.

Let the corresponding perturbation vector be

$$\boldsymbol{\omega} = (\boldsymbol{\alpha}_1^\top, \dots, \boldsymbol{\alpha}_K^\top, \delta_1, \dots, \delta_K, \gamma_1, \dots, \gamma_K, \iota)^\top \in \mathbb{R}^N,$$

where $\boldsymbol{\alpha}_k \in \mathbb{R}^m$ corresponds to \mathbf{w}_k , $\delta_k \in \mathbb{R}$ to b_k , $\gamma_k \in \mathbb{R}$ to v_k , and $\iota \in \mathbb{R}$ to β . The normalization constraint is

$$\|\boldsymbol{\omega}\|_2^2 = \sum_{k=1}^K \|\boldsymbol{\alpha}_k\|_2^2 + \sum_{k=1}^K \delta_k^2 + \sum_{k=1}^K \gamma_k^2 + \iota^2 = 1.$$

For the fixed input \mathbf{x} , set $\mathbf{x}^{(S_j)} := \pi_j(\mathbf{x}) \in \mathbb{R}^m$ and define the ReLU gate

$$m_k^{(S_j)} := \mathbf{1}\{\mathbf{w}_k^\top \mathbf{x}^{(S_j)} > b_k\} \in \{0, 1\}.$$

By the twice-differentiability assumption, all gates are constant in a neighborhood of $\boldsymbol{\theta}$.

Within this gate-fixed region, f_θ is affine in (\mathbf{w}_k, b_k) once v_k is held fixed, and affine in v_k once (\mathbf{w}_k, b_k) are held fixed. Therefore the only nonzero second partial derivatives inside the k -th neuron block are the mixed ones with v_k

$$\frac{\partial^2 f_\theta}{\partial \mathbf{w}_k \partial v_k} = \frac{\partial}{\partial v_k} \left(\frac{1}{J} \sum_{S_j \in \mathcal{S}} v_k m_k^{(S_j)} \mathbf{x}^{(S_j)} \right) = \frac{1}{J} \sum_{j=1}^J m_k^{(S_j)} \mathbf{x}^{(S_j)} =: \mathbf{s}_k \in \mathbb{R}^m, \quad (36)$$

$$\frac{\partial^2 f_\theta}{\partial b_k \partial v_k} = \frac{\partial}{\partial v_k} \left(\frac{1}{J} \sum_{j=1}^J v_k m_k^{(S_j)} \right) = \frac{1}{J} \sum_{j=1}^J m_k^{(S_j)} =: t_k \in \mathbb{R}. \quad (37)$$

All other second derivatives inside the block vanish (as do any cross-neuron second derivatives and all those involving β). Hence, with the block variable $\theta_k := (\mathbf{w}_k^\top, b_k, v_k)^\top$, we have

$$\nabla_{(\theta_k)}^2 f_\theta(\mathbf{x}) = \begin{pmatrix} \mathbf{0}_{k \times k} & \mathbf{0}_k & \mathbf{s}_k \\ \mathbf{0}_k^\top & 0 & t_k \\ \mathbf{s}_k^\top & t_k & 0 \end{pmatrix}. \quad (38)$$

The full quadratic form splits over neuron blocks:

$$\begin{aligned} \boldsymbol{\omega}^\top \nabla_{\boldsymbol{\theta}}^2 f_\theta(\mathbf{x}) \boldsymbol{\omega} &= \sum_{k=1}^K (\boldsymbol{\alpha}_k^\top \quad \delta_k \quad \gamma_k) \begin{pmatrix} \mathbf{0} & \mathbf{0} & \mathbf{s}_k \\ \mathbf{0}^\top & 0 & t_k \\ \mathbf{s}_k^\top & t_k & 0 \end{pmatrix} \begin{pmatrix} \boldsymbol{\alpha}_k \\ \delta_k \\ \gamma_k \end{pmatrix} \\ &= \sum_{k=1}^K 2\gamma_k (\boldsymbol{\alpha}_k^\top \mathbf{s}_k + \delta_k t_k). \end{aligned} \quad (39)$$

Recall the definition of the notations (36) and (37),

$$t_k = \frac{1}{J} \sum_{j=1}^J m_k^{(S_j)} \leq 1, \quad (40)$$

$$\|\mathbf{s}_k\|_2 = \left\| \frac{1}{J} \sum_{j=1}^J m_k^{(S_j)} \mathbf{x}^{(S_j)} \right\|_2 \leq \frac{1}{J} \sum_{j=1}^J m_k^{(S_j)} \|\mathbf{x}^{(S_j)}\|_2 \leq \frac{1}{J} \sum_{j=1}^J m_k^{(S_j)} R = R t_k, \quad (41)$$

because $\mathbf{x}^{(S_j)} = \pi_j(\mathbf{x})$ is a coordinate projection of \mathbf{x} , $\|\mathbf{x}^{(S_j)}\|_2 \leq \|\mathbf{x}\|_2 \leq R$.

Then for each k ,

$$|2\gamma_k(\boldsymbol{\alpha}_k^\top \mathbf{s}_k + \delta_k t_k)| \leq 2|\gamma_k| \left(\|\boldsymbol{\alpha}_k\|_2 \|\mathbf{s}_k\|_2 + |\delta_k| t_k \right) \quad (\text{Cauchy-Schwarz})$$

$$(41) \implies \leq 2|\gamma_k| \left(R t_k \|\boldsymbol{\alpha}_k\|_2 + |\delta_k| t_k \right)$$

$$(40) \implies \leq 2|\gamma_k| \left(R \|\boldsymbol{\alpha}_k\|_2 + |\delta_k| \right), \quad (42)$$

Summing over k for (42) and plug in (39), we have

$$\begin{aligned} |\boldsymbol{\omega}^\top \nabla_{\boldsymbol{\theta}}^2 f_{\boldsymbol{\theta}}(\mathbf{x}) \boldsymbol{\omega}| &\leq 2 \left(R \sum_k |\gamma_k| \|\boldsymbol{\alpha}_k\|_2 + \sum_k |\gamma_k| |\delta_k| \right) \\ (\text{Cauchy-Schwarz}) &\leq 2 \left(R \sqrt{\sum_k \gamma_k^2} \sqrt{\sum_k \|\boldsymbol{\alpha}_k\|_2^2} + \sqrt{\sum_k \gamma_k^2} \sqrt{\sum_k \delta_k^2} \right). \end{aligned} \quad (43)$$

Using the normalization $\sum_k \|\boldsymbol{\alpha}_k\|_2^2 + \sum_k \delta_k^2 + \sum_k \gamma_k^2 + t^2 = 1$, we have $\sqrt{\sum_k \gamma_k^2} \leq 1$, $\sqrt{\sum_k \|\boldsymbol{\alpha}_k\|_2^2} \leq 1$, and $\sqrt{\sum_k \delta_k^2} \leq 1$. Thus $|\boldsymbol{\omega}^\top \nabla_{\boldsymbol{\theta}}^2 f_{\boldsymbol{\theta}}(\mathbf{x}) \boldsymbol{\omega}| \leq 2(R+1)$. \square

Theorem B.4 (Restate Theorem 4.1). *Given a data set $\mathcal{D} = \{\mathbf{x}_i, y_i\}_{i=1}^n$ and a network model (1) with the set of local receptive fields \mathcal{S} , we have*

$$\sum_{k=1}^K |v_k| \|\mathbf{w}_k\| g_{\mathcal{D}, \mathcal{S}} \left(\frac{\mathbf{w}_k}{\|\mathbf{w}_k\|}, \frac{b_k}{\|\mathbf{w}_k\|} \right) \leq \frac{1}{2} \left(\lambda_{\max}(\nabla_{\boldsymbol{\theta}}^2 \mathcal{L}(\boldsymbol{\theta})) + 2(R+1)\sqrt{2\mathcal{L}(\boldsymbol{\theta})} - 1 \right).$$

Proof. It suffices to prove the first assertion. Recall that by direct computation, the Hessian matrix of the loss function is expressed as

$$\nabla_{\boldsymbol{\theta}}^2 \mathcal{L} = \underbrace{\frac{1}{n} \sum_{i=1}^n \nabla_{\boldsymbol{\theta}} f(\mathbf{x}_i) \nabla_{\boldsymbol{\theta}} f(\mathbf{x}_i)^\top}_{\mathbf{T}_{\mathcal{D}}} + \underbrace{\frac{1}{n} \sum_{i=1}^n (f(\mathbf{x}_i) - y_i) \nabla_{\boldsymbol{\theta}}^2 f(\mathbf{x}_i)}_{\mathbf{R}_{\mathcal{D}}}. \quad (44)$$

Let $\boldsymbol{\omega}$ be the unit eigenvector (i.e., $\|\boldsymbol{\omega}\|_2 = 1$) corresponding to the largest eigenvalue of the matrix $\mathbf{T}_{\mathcal{D}}$, the maximum eigenvalue of the Hessian matrix of the loss can be lower-bounded as follows:

$$\begin{aligned} \lambda_{\max}(\nabla_{\boldsymbol{\theta}}^2 \mathcal{L}(\boldsymbol{\theta})) &\geq \boldsymbol{\omega}^\top \nabla_{\boldsymbol{\theta}}^2 \mathcal{L}(\boldsymbol{\theta}) \boldsymbol{\omega} \\ &\geq \underbrace{\lambda_{\max}(\mathbf{T}_{\mathcal{D}})}_{(\text{Term A})} + \underbrace{\frac{1}{n} \sum_{i=1}^n (f_{\boldsymbol{\theta}}(\mathbf{x}_i) - y_i) \boldsymbol{\omega}^\top \nabla_{\boldsymbol{\theta}}^2 f_{\boldsymbol{\theta}}(\mathbf{x}_i) \boldsymbol{\omega}}_{(\text{Term B})}. \end{aligned} \quad (45)$$

According to Proposition B.2, Term A is lower bounded by

$$\lambda_{\max}(\mathbf{T}_{\mathcal{D}}) \geq 1 + 2 \sum_{k=1}^K |v_k| \|\mathbf{w}_k\| g_{\mathcal{D}, \mathcal{S}} \left(\frac{\mathbf{w}_k}{\|\mathbf{w}_k\|}, \frac{b_k}{\|\mathbf{w}_k\|} \right), \quad (46)$$

For (Term B), an upper bound can be established using the training loss $\mathcal{L}(\boldsymbol{\theta})$ via the Cauchy-Schwarz inequality. This also employs a notable uniform upper bound for $|\boldsymbol{\omega}^\top \nabla_{\boldsymbol{\theta}}^2 f_{\boldsymbol{\theta}}(\mathbf{x}_n) \boldsymbol{\omega}|$, as detailed in Lemma B.3:

$$|(\text{Term B})| \leq \sqrt{\frac{1}{n} \sum_{i=1}^n (f_{\boldsymbol{\theta}}(\mathbf{x}_i) - y_i)^2} \cdot \sqrt{\frac{1}{n} \sum_{i=1}^n (\boldsymbol{\omega}^\top \nabla_{\boldsymbol{\theta}}^2 f_{\boldsymbol{\theta}}(\mathbf{x}_i) \boldsymbol{\omega})^2} \leq 2(R+1)\sqrt{2\mathcal{L}(\boldsymbol{\theta})}. \quad (47)$$

Thus, we have

$$\lambda_{\max}(\mathbf{T}_{\mathcal{D}}) \leq \lambda_{\max}(\nabla_{\boldsymbol{\theta}}^2 \mathcal{L}(\boldsymbol{\theta})) + |(\text{Term B})| \leq \lambda_{\max}(\nabla_{\boldsymbol{\theta}}^2 \mathcal{L}(\boldsymbol{\theta})) + 2(R+1)\sqrt{2\mathcal{L}(\boldsymbol{\theta})}. \quad (48)$$

Finally, we plug (46) into (48)

$$\sum_{k=1}^K |v_k| \|\mathbf{w}_k\| g_{\mathcal{D},S} \left(\frac{\mathbf{w}_k}{\|\mathbf{w}_k\|}, \frac{b_k}{\|\mathbf{w}_k\|} \right) \leq \frac{1}{2} \left(\lambda_{\max}(\nabla_{\boldsymbol{\theta}}^2 \mathcal{L}(\boldsymbol{\theta})) + 2(R+1)\sqrt{2\mathcal{L}(\boldsymbol{\theta})} - 1 \right).$$

□

B.1. Empirical Process for the Weight Function

We study uniform deviations of the empirical weight function $g_{\mathcal{D},S}$ from its population counterpart $g_{\mathcal{P},S}$ under i.i.d. sampling $\mathbf{x}_1, \dots, \mathbf{x}_n \sim \mathcal{P}_{\mathbf{X}}$. Although the collection $\{\pi_j(\mathbf{x}_i)\}_{i,j}$ is not i.i.d. across (i, j) in general, for each fixed j the patches $\{\pi_j(\mathbf{x}_i)\}_{i=1}^n$ are i.i.d. in \mathbb{R}^m .

Definition B.5. For any $S_j \in \mathcal{S}$, let $\mathbf{X}_{\mathcal{D}}^{(S_j)}$ be a random vector drawn uniformly at random from the training examples $\{\pi_j(\mathbf{x}_i)\}_{i=1}^n$ with patch extraction to the local receptive field S_j . For any $\mathbf{u} \in \mathbb{S}^{m-1}$, $t \in \mathbb{R}$, define the aggregated gate probability, ReLU margin, and gated first moment

$$\begin{aligned} \bar{p}_{\mathcal{D},S}(\mathbf{u}, t) &:= \frac{1}{J} \sum_{j=1}^J \mathbb{P} \left(\mathbf{u}^{\top} \mathbf{X}_{\mathcal{D}}^{(S_j)} > t \right), \\ \bar{r}_{\mathcal{D},S}(\mathbf{u}, t) &:= \frac{1}{J} \sum_{j=1}^J \mathbb{E} \left[\phi \left(\mathbf{u}^{\top} \mathbf{X}_{\mathcal{D}}^{(S_j)} - t \right) \right], \\ \bar{\mathbf{a}}_{\mathcal{D},S}(\mathbf{u}, t) &:= \frac{1}{J} \sum_{j=1}^J \mathbb{E} \left[\mathbf{X}_{\mathcal{D}}^{(S_j)} \mathbf{1} \left\{ \mathbf{u}^{\top} \mathbf{X}_{\mathcal{D}}^{(S_j)} > t \right\} \right] \in \mathbb{R}^m. \end{aligned} \quad (49)$$

Base on these terminologies, we may rewrite the weight function

$$\tilde{g}_{\mathcal{D},S}(\mathbf{u}, t) := \bar{r}_{\mathcal{D},S}(\mathbf{u}, t) \sqrt{\bar{p}_{\mathcal{D},S}(\mathbf{u}, t)^2 + \|\bar{\mathbf{a}}_{\mathcal{D},S}(\mathbf{u}, t)\|_2^2}. \quad (50)$$

For each $j \in [J]$ and $(\mathbf{u}, t) \in \mathbb{S}^{m-1} \times [-1, 1]$, define the population components

$$p_j(\mathbf{u}, t) := \mathbb{P}(\mathbf{u}^{\top} \pi_j(\mathbf{X}) > t), \quad r_j(\mathbf{u}, t) := \mathbb{E}[\phi(\mathbf{u}^{\top} \pi_j(\mathbf{X}) - t)], \quad \mathbf{a}_j(\mathbf{u}, t) := \mathbb{E}[\pi_j(\mathbf{X}) \mathbf{1}\{\mathbf{u}^{\top} \pi_j(\mathbf{X}) > t\}],$$

and their averages $\bar{p}_{\mathcal{P},S}, \bar{r}_{\mathcal{P},S}, \bar{\mathbf{a}}_{\mathcal{P},S}$ as in (49). Then

$$\tilde{g}_{\mathcal{P},S}(\mathbf{u}, t) = \bar{r}_{\mathcal{P},S}(\mathbf{u}, t) \sqrt{\bar{p}_{\mathcal{P},S}(\mathbf{u}, t)^2 + \|\bar{\mathbf{a}}_{\mathcal{P},S}(\mathbf{u}, t)\|_2^2}, \quad g_{\mathcal{P},S}(\mathbf{u}, t) = \min\{\tilde{g}_{\mathcal{P},S}(\mathbf{u}, t), \tilde{g}_{\mathcal{P},S}(-\mathbf{u}, -t)\}.$$

Theorem B.6 (Uniform deviation for $g_{\mathcal{D},S}$). *Assume $\|\pi_j(\mathbf{X})\|_2 \leq 1$ almost surely for all $j \in [J]$. There exists a universal constant $C > 0$ such that for every $\delta \in (0, 1)$, with probability at least $1 - \delta$,*

$$\sup_{\mathbf{u} \in \mathbb{S}^{m-1}, t \in [-1, 1]} |\tilde{g}_{\mathcal{D},S}(\mathbf{u}, t) - \tilde{g}_{\mathcal{P},S}(\mathbf{u}, t)| \leq C_{\text{ep}} \sqrt{\frac{m + \log(2J/\delta)}{n}}.$$

Consequently (since $\min(\cdot, \cdot)$ is 1-Lipschitz),

$$\sup_{\mathbf{u} \in \mathbb{S}^{m-1}, t \in [-1, 1]} |g_{\mathcal{D},S}(\mathbf{u}, t) - g_{\mathcal{P},S}(\mathbf{u}, t)| \leq C_{\text{ep}} \sqrt{\frac{m + \log(2J/\delta)}{n}}.$$

Proof. We bound $\hat{p} - \bar{p}$, $\hat{r} - \bar{r}$, and $\hat{\mathbf{a}} - \bar{\mathbf{a}}$ uniformly and then combine them by a Lipschitz argument.

For each fixed j , the class $\{z \mapsto \mathbf{1}\{\mathbf{u}^{\top} z > t\} : \mathbf{u} \in \mathbb{S}^{m-1}, t \in \mathbb{R}\}$ on \mathbb{R}^m has VC-dimension $m + 1$, so VC uniform convergence yields

$$\sup_{\mathbf{u}, t \in [-1, 1]} |\hat{p}_j(\mathbf{u}, t) - p_j(\mathbf{u}, t)| \lesssim \sqrt{\frac{m + \log(1/\delta)}{n}}$$

with probability at least $1 - \delta$. Similarly, the ReLU class $\{(\mathbf{u}^\top \mathbf{z} - t)_+ : \mathbf{u} \in \mathbb{S}^{m-1}, t \in [-1, 1]\}$ has pseudo-dimension $O(m)$, hence

$$\sup_{\mathbf{u}, t \in [-1, 1]} |\hat{r}_j(\mathbf{u}, t) - r_j(\mathbf{u}, t)| \lesssim \sqrt{\frac{m + \log(1/\delta)}{n}}$$

with probability at least $1 - \delta$. Finally, for the vector moment, apply the same VC-type bound coordinate-wise to the bounded class $\mathbf{z} \mapsto z_\ell \mathbb{1}\{\mathbf{u}^\top \mathbf{z} > t\}$ (bounded by 1 in absolute value under $\|\mathbf{z}\| \leq 1$), and take a union bound over $\ell \in [m]$ to get

$$\sup_{\mathbf{u}, t \in [-1, 1]} \|\hat{\mathbf{a}}_j(\mathbf{u}, t) - \mathbf{a}_j(\mathbf{u}, t)\|_2 \lesssim \sqrt{\frac{m + \log(1/\delta)}{n}}$$

with probability at least $1 - \delta$.

A union bound over $j \in [J]$ upgrades the above bounds simultaneously for all j with failure probability δ , producing the log J term. Averaging over j does not increase the sup norm, so the same rate holds for $(\tilde{p}, \tilde{r}, \tilde{\mathbf{a}})$.

Now use the deterministic bounds $0 \leq \bar{r} \leq 2$, $0 \leq \bar{p} \leq 1$, and $\|\bar{\mathbf{a}}\| \leq \bar{p}$ (since $\|\pi_j(\mathbf{X})\| \leq 1$) to show the map

$$(\bar{r}, \bar{p}, \bar{\mathbf{a}}) \mapsto \bar{r} \sqrt{\bar{p}^2 + \|\bar{\mathbf{a}}\|^2}$$

is Lipschitz on this bounded domain. Hence the stated uniform deviation for \tilde{g} follows. The claim for g follows from the 1-Lipschitz property of $\min(\cdot, \cdot)$:

$$|\min\{A, B\} - \min\{A', B'\}| \leq \max\{|A - A'|, |B - B'|\}.$$

□

B.2. The Computation of the Population Weight Function for Uniform(\mathbb{S}^{d-1})

Assume that $\mathcal{P}_{\mathbf{X}}$ is a uniform distribution on $\mathbb{S}^{d-1} \subset \mathbb{R}^d$. Here we compute the population version of the components in the weighted function $g_{\mathcal{D}, \mathcal{S}}$ defined in Definition B.5.

Let $d \geq 2$, $m < d$. Draw $\mathbf{X} \sim \text{Uniform}(\mathbb{S}^{d-1}) \subset \mathbb{R}^d$, set $\mathbf{Z} = \text{proj}(\mathbf{X}) \in \mathbb{R}^m$ by projecting the first m coordinates, and fix any unit $\mathbf{u} \in \mathbb{R}^m$. Define

$$Z := \mathbf{u}^\top \mathbf{Z} \in [-1, 1]. \quad (51)$$

By rotational invariance in \mathbb{R}^d , Z has the one-coordinate marginal of $\text{Uniform}(\mathbb{S}^{d-1})$, hence its density is

$$f_d(z) = c_d (1 - z^2)^{\frac{d-3}{2}} \mathbb{1}\{-1 \leq z \leq 1\}, \quad c_d := \frac{\Gamma(\frac{d}{2})}{\sqrt{\pi} \Gamma(\frac{d-1}{2})}. \quad (52)$$

All bounds below are independent of m and \mathbf{u} , depending only on d .

For shorthand, write $\alpha := \frac{d-3}{2} \geq -\frac{1}{2}$ and observe

$$(1 - z^2)^\alpha = [(1 - z)(1 + z)]^\alpha, \quad z \in [-1, 1], \quad (53)$$

together with the elementary bounds $1 \leq 1 + z \leq 2$ for $z \in [0, 1]$.

Lemma B.7 ((Tail of Z)). *For all $t \in [0, 1)$,*

$$\frac{c_d}{\alpha + 1} (1 - t)^{\alpha+1} \leq \mathbb{P}(Z > t) \leq \frac{c_d 2^\alpha}{\alpha + 1} (1 - t)^{\alpha+1}. \quad (54)$$

Consequently $\mathbb{P}(Z > t) \asymp (1 - t)^{\frac{d-1}{2}}$ as $t \rightarrow 1^-$.

Proof. Using (52) and (53),

$$\mathbb{P}(Z > t) = \int_t^1 c_d (1 - z^2)^\alpha dz = c_d \int_t^1 [(1 - z)(1 + z)]^\alpha dz. \quad (55)$$

Since $1 \leq 1 + z \leq 2$ for $z \in [t, 1]$, we have

$$c_d \int_t^1 (1-z)^\alpha dz \leq \mathbb{P}(Z > t) \leq c_d 2^\alpha \int_t^1 (1-z)^\alpha dz. \quad (56)$$

Evaluating $\int_t^1 (1-z)^\alpha dz = \frac{(1-t)^{\alpha+1}}{\alpha+1}$ (valid for $\alpha > -1$; here $\alpha \geq -\frac{1}{2}$), we obtain (54). \square

Lemma B.8. For all $t \in [0, 1)$,

$$\frac{c_d}{(\alpha+1)(\alpha+2)} (1-t)^{\alpha+2} \leq \mathbb{E}[\phi(Z-t)] \leq \frac{c_d 2^\alpha}{(\alpha+1)(\alpha+2)} (1-t)^{\alpha+2}. \quad (57)$$

Consequently $\mathbb{E}[\phi(Z-t)] \asymp (1-t)^{\frac{d+1}{2}}$ as $t \uparrow 1$.

Proof. By definition and (52),

$$\mathbb{E}[\phi(Z-t)] = \int_t^1 (z-t) f_d(z) dz = c_d \int_t^1 (z-t) [(1-z)(1+z)]^\alpha dz. \quad (58)$$

Bounding $1 \leq 1+z \leq 2$ for $z \in [t, 1]$ yields

$$c_d \int_t^1 (z-t)(1-z)^\alpha dz \leq \mathbb{E}[\phi(Z-t)] \leq c_d 2^\alpha \int_t^1 (z-t)(1-z)^\alpha dz. \quad (59)$$

Substitute $y = 1-z$ to compute the shared integral:

$$\int_t^1 (z-t)(1-z)^\alpha dz = \int_0^{1-t} [(1-t)-y] y^\alpha dy = \frac{(1-t)^{\alpha+2}}{(\alpha+1)(\alpha+2)}, \quad (60)$$

valid for $\alpha > -1$. This gives (57). \square

Proposition B.9. There exist absolute constants (depending only on d)

$$c_L(d) := \frac{c_d^2}{(\alpha+1)^2(\alpha+2)}, \quad c_U(d) := \frac{c_d^2 2^{2\alpha}}{(\alpha+1)^2(\alpha+2)}, \quad (61)$$

such that for all $t \in [0, 1)$,

$$c_L(d) (1-t)^{2\alpha+3} \leq \mathbb{P}(Z > t) \cdot \mathbb{E}[\phi(Z-t)] \leq c_U(d) (1-t)^{2\alpha+3}. \quad (62)$$

Equivalently, since $\alpha = \frac{d-3}{2}$,

$$\mathbb{P}(Z > t) \cdot \mathbb{E}[\phi(Z-t)] \asymp (1-t)^d \quad \text{as } t \uparrow 1, \quad (63)$$

with explicit

$$c_L(d) = \frac{c_d^2}{\left(\frac{d-1}{2}\right)^2 \left(\frac{d+1}{2}\right)}, \quad c_U(d) = \frac{c_d^2 2^{d-3}}{\left(\frac{d-1}{2}\right)^2 \left(\frac{d+1}{2}\right)}, \quad c_d = \frac{\Gamma\left(\frac{d}{2}\right)}{\sqrt{\pi} \Gamma\left(\frac{d-1}{2}\right)}. \quad (64)$$

Proof. The inequality can be deduced by combining (54) and (57). \square

Proposition B.10 (Boundary tail for projected radius). Fix integers $d \geq 2$ and $1 \leq m < d$. Let $\mathbf{X} \sim \text{Uniform}(\mathbb{S}^{d-1}) \subset \mathbb{R}^d$ and $\mathbf{Z} = \text{proj}(\mathbf{X}) \in \mathbb{R}^m$. Then there exist universal constants

$$c_L(d, m), c_U(d, m) \in (0, \infty)$$

depending only on d, m (and independent of the choice of projection and of t) such that for all $t \in (0, \frac{1}{4}]$,

$$c_L(d, m) t^{\frac{d-m}{2}} \leq \mathbb{P}(\|\mathbf{Z}\| > 1-t) \leq c_U(d, m) t^{\frac{d-m}{2}}. \quad (65)$$

In particular,

$$\mathbb{P}(\|\mathbf{Z}\| > 1 - t) \asymp t^{\frac{d-m}{2}} \quad \text{as } t \downarrow 0, \quad (66)$$

with one admissible choice

$$c_L(d, m) = \frac{2^{-|\frac{m}{2}-1|}}{\frac{d-m}{2} B(\frac{m}{2}, \frac{d-m}{2})}, \quad c_U(d, m) = \frac{2^{|\frac{m}{2}-1|+\frac{d-m}{2}}}{\frac{d-m}{2} B(\frac{m}{2}, \frac{d-m}{2})}, \quad (67)$$

where $B(a, b) = \Gamma(a)\Gamma(b)/\Gamma(a+b)$ denotes the Beta function.

Proof. Write $R := \|\mathbf{Z}\| \in [0, 1]$ and $S := R^2$. A standard Gaussian-ratio representation gives

$$S \sim \text{Beta}(a, b), \quad a := \frac{m}{2}, \quad b := \frac{d-m}{2}, \quad (68)$$

with density

$$f_S(x) = \frac{x^{a-1}(1-x)^{b-1}}{B(a, b)} \mathbf{1}_{\{0 < x < 1\}}. \quad (69)$$

For $t \in (0, 1)$,

$$\mathbb{P}(R > 1 - t) = \mathbb{P}(S > (1 - t)^2) = \frac{1}{B(a, b)} \int_{(1-t)^2}^1 x^{a-1}(1-x)^{b-1} dx. \quad (70)$$

Set $y := 1 - (1 - t)^2 = 2t - t^2$. Then $y \in (0, 2t)$ and for $t \in (0, \frac{1}{4}]$ we have $y \leq \frac{1}{2}$ and $(1 - y) \geq \frac{1}{2}$. Since $x \in [1 - y, 1]$, the elementary bound

$$2^{-|a-1|} \leq x^{a-1} \leq 2^{|a-1|} \quad \text{for all } x \in [\frac{1}{2}, 1] \quad (71)$$

holds deterministically (because $\ln x \in [-\ln 2, 0]$ and $x^{a-1} = e^{(a-1)\ln x}$). Using (71) in (70) and integrating the $(1-x)^{b-1}$ part exactly gives

$$\frac{2^{-|a-1|}}{B(a, b)} \int_{1-y}^1 (1-x)^{b-1} dx \leq \mathbb{P}(R > 1 - t) \leq \frac{2^{|a-1|}}{B(a, b)} \int_{1-y}^1 (1-x)^{b-1} dx. \quad (72)$$

Since $\int_{1-y}^1 (1-x)^{b-1} dx = \frac{y^b}{b}$, we obtain

$$\frac{2^{-|a-1|}}{b B(a, b)} y^b \leq \mathbb{P}(R > 1 - t) \leq \frac{2^{|a-1|}}{b B(a, b)} y^b. \quad (73)$$

Finally, because $t \leq y \leq 2t$, we have $t^b \leq y^b \leq (2t)^b$, and (73) yields

$$\frac{2^{-|a-1|}}{b B(a, b)} t^b \leq \mathbb{P}(R > 1 - t) \leq \frac{2^{|a-1|+b}}{b B(a, b)} t^b, \quad (74)$$

which is exactly (65) with the explicit constants in (67). This proves $\mathbb{P}(\|\mathbf{Z}\| > 1 - t) \asymp t^b = t^{(d-m)/2}$ as $t \downarrow 0$. \square

C. Proof of Theorem 4.2

Theorem C.1 (Detailed version of Theorem 4.2). *Suppose \mathcal{P} is a joint distribution of (\mathbf{x}, y) . Assume that the marginal distribution of \mathbf{x} is Uniform(\mathbb{S}^{d-1}) and the marginal distribution of y is supported on $[-D, D]$ for some $D > 0$. Fix a dataset $\mathcal{D} = \{(\mathbf{x}_i, y_i)\}_{i=1}^n$, where each data point is drawn i.i.d. from \mathcal{P} . Let $M \geq D$. If $\boldsymbol{\theta} \in \Theta_{\text{BEoS}}^{\text{S}}(\eta, \mathcal{D})$ and $\|f_{\boldsymbol{\theta}}\|_{\infty} \leq M$, then, with probability $\geq 1 - 2\delta$, we have that for the plug-in risk estimator $\widehat{R}_{\mathcal{D}}(f) := \frac{1}{n} \sum_{i=1}^n (f(\mathbf{x}_i) - y_i)^2$,*

$$\left| \mathbb{E}_{(\mathbf{x}, y) \sim \mathcal{P}} \left[(f_{\boldsymbol{\theta}}(\mathbf{x}) - y)^2 \right] - \widehat{R}_{\mathcal{D}}(f_{\boldsymbol{\theta}}) \right| \lesssim_d JM^2 \varepsilon^{\frac{d-m}{2}} + \left(\frac{A}{J} \varepsilon^{-d} \right)^{\frac{d}{d+3}} M^{\frac{3(d+2)}{2d+3}} n^{-\frac{1}{2}}, \quad (75)$$

for any $\varepsilon \in (0, 1)$ such that $\varepsilon^d \gtrsim d^2 \sqrt{\frac{m + \log(J/\delta)}{n}}$. Here $A = \frac{1}{\eta} - 1 + 4M$, and \lesssim_d hides constants depending only on d and logarithmic factors in n and (J/δ) .

Proof. For $\varepsilon \in (0, 1)$, we define

$$\mathbb{I}_\varepsilon^{\text{all}} := \left\{ \mathbf{x} \in \mathbb{S}^{d-1} : \max_{S_j \in \mathcal{S}} \|\mathbf{x}^{(S_j)}\| \leq 1 - \varepsilon \right\}, \quad (76)$$

$$\mathbb{O}_\varepsilon^{\text{any}} := \left\{ \mathbf{x} \in \mathbb{S}^{d-1} : \exists S_j \in \mathcal{S}, \|\mathbf{x}^{(S_j)}\| > 1 - \varepsilon \right\}. \quad (77)$$

Then $\mathbb{S}^{d-1} = \mathbb{I}_\varepsilon^{\text{all}} \cup \mathbb{O}_\varepsilon^{\text{any}}$ (disjoint). According to the law of total expectation, the population risk is decomposed into

$$\mathbb{E}_{(\mathbf{x}, y) \sim \mathcal{P}} \left[(f(\mathbf{x}) - y)^2 \right] = \mathbb{P}(\mathbf{x} \in \mathbb{O}_\varepsilon^{\text{any}}) \cdot \mathbb{E}_{\mathbb{O}} \left[(f(\mathbf{x}) - y)^2 \right] + \mathbb{P}(\mathbf{x} \in \mathbb{I}_\varepsilon^{\text{all}}) \cdot \mathbb{E}_{\mathbb{I}} \left[(f(\mathbf{x}) - y)^2 \right], \quad (78)$$

where $\mathbb{E}_{\mathbb{O}}$ means that $\{\mathbf{x}, y\}$ is a new sample from the data distribution conditioned on $\mathbf{x} \in \mathbb{O}_\varepsilon^{\text{any}}$ and $\mathbb{E}_{\mathbb{I}}$ means that (\mathbf{x}, y) is a new sample from the data distribution conditioned on $\mathbf{x} \in \mathbb{I}_\varepsilon^{\text{all}}$.

Similarly, we also have this decomposition for empirical risk

$$\begin{aligned} \frac{1}{n} \sum_{i=1}^n (f(\mathbf{x}_i) - y_i)^2 &= \frac{1}{n} \left(\sum_{i \in I} (f(\mathbf{x}_i) - y_i)^2 + \sum_{i \in O} (f(\mathbf{x}_i) - y_i)^2 \right) \\ &= \frac{n_I}{n} \frac{1}{n_I} \sum_{i \in I} (f(\mathbf{x}_i) - y_i)^2 + \frac{n_O}{n} \frac{1}{n_O} \sum_{i \in O} (f(\mathbf{x}_i) - y_i)^2, \end{aligned} \quad (79)$$

where I is the set of data points with $\mathbf{x}_i \in \mathbb{I}_\varepsilon^{\text{all}}$ and O is the set of data points with $\mathbf{x}_i \in \mathbb{O}_\varepsilon^{\text{any}}$. Then the generalization gap can be decomposed into

$$|R(f) - \hat{R}_{\mathcal{D}}(f)| \leq \mathbb{P}(\mathbf{x} \in \mathbb{O}_\varepsilon^{\text{any}}) \cdot \mathbb{E}_{\mathbb{O}} \left[(f_{\theta}(\mathbf{x}) - y)^2 \right] + \frac{n_O}{n} \frac{1}{n_O} \sum_{i \in O} (f(\mathbf{x}_i) - y_i)^2 \quad (80)$$

$$+ \left| \mathbb{P}(\mathbf{x} \in \mathbb{I}_\varepsilon^{\text{all}}) - \frac{n_I}{n} \right| \frac{1}{n_I} \sum_{i \in I} (f(\mathbf{x}_i) - y_i)^2 \quad (81)$$

$$+ \mathbb{P}(\mathbf{x} \in \mathbb{I}_\varepsilon^{\text{all}}) \cdot \left| \mathbb{E}_{\mathbb{I}} \left[(f(\mathbf{x}) - y)^2 \right] - \frac{1}{n_I} \sum_{i \in I} (f(\mathbf{x}_i) - y_i)^2 \right|. \quad (82)$$

Using the property that the marginal distribution of \mathbf{x} is Uniform(\mathbb{S}^{d-1}) and its concentration property (Proposition B.10 + union bound),

$$\mathbb{P}(\mathbb{O}_\varepsilon^{\text{any}}) = \mathbb{P} \left(\bigcup_{S_j \in \mathcal{S}} \{\|\mathbf{x}^{(S_j)}\| > 1 - \varepsilon\} \right) \lesssim_d J \cdot \varepsilon^{\frac{d-m}{2}}. \quad (83)$$

The Hoeffding inequality guarantees that, with probability at least $1 - \delta/3$,

$$\frac{n_O}{n} \leq J \cdot \varepsilon^{\frac{d-m}{2}} + \sqrt{\frac{\log(6/\delta)}{n}} \quad (84)$$

Therefore, we may conclude that

$$(80) \lesssim_d JM^2 \varepsilon^{\frac{d-m}{2}}, \quad (85)$$

where \lesssim_d hides the constants that could depend on d and logarithmic factors of $1/\delta$.

For the term (81), with probability $1 - \delta/3$

$$\begin{cases} \left| \mathbb{P}(\mathbf{x} \in \mathbb{I}_\varepsilon^{\text{all}}) - \frac{n_I}{n} \right| & \lesssim \sqrt{\frac{\varepsilon^{(d-m)/2} \log(6J/\delta)}{n}}, \\ \frac{1}{n_I} \sum_{i \in I} (f(\mathbf{x}_i) - y_i)^2 & \lesssim M^2 \end{cases} \quad (86)$$

¹We only need $\text{poly}(d)$ samples to make the feasible choice of ε non-vacuous. Here we hide the universal constant.

so we may also conclude that

$$(81) \lesssim M^2 \sqrt{\frac{\varepsilon^{(d-m)/2} \log(6J/\delta)}{n}} \leq M^2 \sqrt{\frac{\log(6J/\delta)}{n}} \quad (87)$$

For the part of the interior (82), the scalar $\mathbb{P}(\mathbf{x} \in \mathbb{I}_\varepsilon^d)$ is less than 1 with high-probability. Therefore, we just need to deal with the term

$$\mathbb{E}_{\mathbb{I}} \left[(f(\mathbf{x}) - y)^2 \right] - \frac{1}{n_I} \sum_{i \in I} (f(\mathbf{x}_i) - y_i)^2. \quad (88)$$

Define the projected core index set $\mathcal{C}_\varepsilon := \{(\mathbf{u}, t) \in \mathbb{S}^{m-1} \times [-1, 1] : |t| \leq 1 - \varepsilon\}$. For any $S_j \in \mathcal{S}$, $\mathbf{X} \sim \text{Uniform}(\mathbb{S}^{d-1})$ and $\mathbf{X}^{(S_j)} = \pi_j(\mathbf{X})$,

- (54) shows that $\mathbb{P}(\mathbf{u}^\top \mathbf{X}^{(S_j)} > t) \asymp (1-t)^{\frac{d-1}{2}}$, and
- (57) shows that $\mathbb{E}[\phi(\mathbf{u}^\top \mathbf{X}^{(S_j)} - t)] \asymp (1-t)^{\frac{d+1}{2}}$.

Therefore we have

$$\left(\frac{1}{J} \sum_{j=1}^J \mathbb{P}(\mathbf{u}^\top \mathbf{X}^{(S_j)} > t) \right) \left(\frac{1}{J} \sum_{j=1}^J \mathbb{E}[\phi(\mathbf{u}^\top \mathbf{X}^{(S_j)} - t)] \right) \asymp (1-t)^d, \quad t \uparrow 1. \quad (89)$$

According to (50) and the definition $g = \min\{\tilde{g}(\mathbf{u}, t), \tilde{g}(-\mathbf{u}, -t)\}$, we have the pointwise lower bound

$$g_{\mathcal{P}, \mathcal{S}}(\mathbf{u}, t) \geq \min \left\{ \bar{r}_{\mathcal{P}, \mathcal{S}}(\mathbf{u}, t) \bar{p}_{\mathcal{P}, \mathcal{S}}(\mathbf{u}, t), \bar{r}_{\mathcal{P}, \mathcal{S}}(-\mathbf{u}, -t) \bar{p}_{\mathcal{P}, \mathcal{S}}(-\mathbf{u}, -t) \right\},$$

since $\sqrt{\bar{p}^2 + \|\bar{\mathbf{a}}\|_2^2} \geq \bar{p}$.

Under $\mathbf{X} \sim \text{Uniform}(\mathbb{S}^{d-1})$, by rotational invariance, for each fixed j and unit \mathbf{u} the quantities $\mathbb{P}(\mathbf{u}^\top \mathbf{X}^{(S_j)} > t)$ and $\mathbb{E}[\phi(\mathbf{u}^\top \mathbf{X}^{(S_j)} - t)]$ depend on t only through the scalar marginal Z in (52). Moreover both are non-increasing in t . Hence the product

$$h(t) := \mathbb{P}(Z > t) \cdot \mathbb{E}[\phi(Z - t)]$$

is non-increasing for $t \in [0, 1)$, and for any $t \in [-1, 1]$ we have

$$g_{\mathcal{P}, \mathcal{S}}(\mathbf{u}, t) \gtrsim_d h(|t|).$$

Therefore, for the core $\mathcal{C}_\varepsilon = \{(\mathbf{u}, t) : |t| \leq 1 - \varepsilon\}$,

$$g_{\mathcal{P}, \mathcal{S}, \min}(\varepsilon) := \inf_{(\mathbf{u}, t) \in \mathcal{C}_\varepsilon} g_{\mathcal{P}, \mathcal{S}}(\mathbf{u}, t) \gtrsim_d h(1 - \varepsilon).$$

By Proposition B.9, $h(1 - \varepsilon) \asymp \varepsilon^d$, hence there exists $c_g(d) > 0$ such that

$$g_{\mathcal{P}, \mathcal{S}, \min}(\varepsilon) \geq c_g(d) \varepsilon^d. \quad (90)$$

On the simultaneous core $\mathbb{I}_\varepsilon^{\text{all}}$, for every local receptive field S_j and any unit $\mathbf{u} \in \mathbb{R}^m$,

$$\|\mathbf{x}^{(S_j)}\| \leq 1 - \varepsilon \Rightarrow \begin{cases} t \geq 1 - \varepsilon \Rightarrow \phi(\mathbf{u}^\top \mathbf{x}^{(S_j)} - t) = 0, \\ t \leq -1 + \varepsilon \Rightarrow \phi(\mathbf{u}^\top \mathbf{x}^{(S_j)} - t) = \mathbf{u}^\top \mathbf{x}^{(S_j)} - t \text{ (affine)}. \end{cases} \quad (91)$$

Therefore all *large-offset* units ($|t| \geq 1 - \varepsilon$) are affine on $\mathbb{I}_\varepsilon^{\text{all}}$ *simultaneously across all views* and can be absorbed into a global affine term. The remaining *core-offset* units with $|t| \leq 1 - \varepsilon$ are controlled by the $g_{\mathcal{S}}$ -weighted variation. Using $|f_\theta|_{V_g} \leq A$ and (90),

$$\left| f_\theta \right|_{V(\mathbb{I}_\varepsilon^{\text{all}})} \leq \frac{|f_\theta|_{V_g}}{g_{\mathcal{P}, \mathcal{S}, \min}(\varepsilon)} \lesssim \frac{A}{J} \varepsilon^{-d}. \quad (92)$$

Therefore, we may leverage the generalization bounds for the unweighted path-norm constraint (see Lemma A.7) to deduce that with probability at least $1 - \delta/3$,

$$(82) \lesssim_d \left(\frac{A}{J} \varepsilon^{-d}\right)^{\frac{d}{d+3}} M^{\frac{d+6}{d+3}} n^{-\frac{1}{2}}, \quad (93)$$

Combining (85), (87) and (93), we obtain

$$\sup_{\boldsymbol{\theta} \in \Theta_{\text{BEoS}}(\eta, \mathcal{D})} \text{Gap}_{\mathcal{P}}(f_{\boldsymbol{\theta}}; \mathcal{D}) \lesssim_d JM^2 \varepsilon^{\frac{d-m}{2}} + \left(\frac{A}{J} \varepsilon^{-d}\right)^{\frac{d}{d+3}} M^{\frac{3(d+2)}{2d+3}} n^{-\frac{1}{2}}. \quad (94)$$

According to standard empirical process theory (see Theorem B.6), for any $\delta \in (0, 1)$, with probability at least $1 - \delta$,

$$\sup_{\substack{\mathbf{u} \in \mathbb{S}^{m-1} \\ t \in [-1, 1]}} |g_{\mathcal{D}, \mathcal{S}}(\mathbf{u}, t) - g_{\mathcal{P}, \mathcal{S}}(\mathbf{u}, t)| \leq C_{\text{ep}} \sqrt{\frac{m + \log(2J/\delta)}{n}} =: \zeta_n. \quad (95)$$

Consequently, for any $\varepsilon \in (0, 1)$,

$$g_{\mathcal{D}, \mathcal{S}, \min}(\varepsilon) := \inf_{\substack{\mathbf{u} \in \mathbb{S}^{m-1} \\ |t| \leq 1 - \varepsilon}} g_{\mathcal{D}, \mathcal{S}}(\mathbf{u}, t) \geq g_{\mathcal{P}, \mathcal{S}, \min}(\varepsilon) - \zeta_n, \quad (96)$$

where $g_{\mathcal{P}, \mathcal{S}, \min}(\varepsilon)$ is the corresponding population quantity.

For $\mathcal{P}_{\mathbf{X}} = \text{Uniform}(\mathbb{S}^{d-1})$, Proposition B.9 (see (65)) gives the explicit lower bound

$$g_{\mathcal{P}, \mathcal{S}, \min}(\varepsilon) \geq c_L(d) \varepsilon^d. \quad (97)$$

Therefore, a sufficient **validity condition** ensuring $g_{\mathcal{D}, \mathcal{S}, \min}(\varepsilon) \geq 2\zeta_n$ is

$$\varepsilon^d \geq \frac{2C_{\text{ep}}}{c_L(d)} \sqrt{\frac{m + \log(2J/\delta)}{n}}. \quad (98)$$

The constant $C_{\text{ep}} > 0$ is universal (it does not depend on d, m, n, J), and can be taken explicitly from any standard VC-/pseudo-dimension uniform convergence inequality; see, e.g., Mohri et al. (2018, Chapter 3) or Haussler (1992). Moreover, the constant $c_L(d)$ defined in Proposition B.9 satisfies

$$c_L(d) \gtrsim \frac{1}{d^2} \quad (d \geq 3), \quad (99)$$

which follows from standard bounds on Gamma-function ratios (e.g. Gautschi's inequality; see dlm, §5.6(i)). Hence the admissible range for ε is nonempty (e.g. $\varepsilon \in [\varepsilon_{\min}, 1)$) as soon as $n \gtrsim \text{poly}(d) (m + \log(2J/\delta))$. \square

Corollary C.2. *Under the same conditions as Theorem 4.2, assume $d > 3$ and $1 \leq m < \frac{d(d-3)}{d+3}$. Let*

$$\mathfrak{N} := (d-m)(d+3) + 2d^2 \quad \text{and} \quad \varepsilon_{\min} := \left(c_d d^2 \sqrt{\frac{m + \log(J/\delta)}{n}} \right)^{1/d}.$$

Define the optimal choice

$$\varepsilon^* \asymp \left(\frac{A^{\frac{d}{d+3}}}{J^{\frac{2d+3}{d+3}} M^{\frac{d}{2d+3}} \sqrt{n}} \right)^{\frac{2(d+3)}{\mathfrak{N}}}, \quad (100)$$

and choose the feasible/truncated value

$$\varepsilon^\dagger := \max\{\varepsilon_{\min}, \varepsilon^*\}.$$

Then, with probability at least $1 - \delta$,

$$\sup_{\boldsymbol{\theta} \in \Theta_{\text{BEoS}}^{\mathcal{S}}(\eta, \mathcal{D})} \left| \mathbb{E}[(f_{\boldsymbol{\theta}}(\mathbf{x}) - y)^2] - \widehat{R}_{\mathcal{D}}(f_{\boldsymbol{\theta}}) \right| \lesssim_d JM^2 (\varepsilon^\dagger)^{\frac{d-m}{2}} + \left(\frac{A}{J} (\varepsilon^\dagger)^{-d}\right)^{\frac{d}{d+3}} M^{\frac{3(d+2)}{2d+3}} n^{-1/2}. \quad (101)$$

Moreover, in the regime where $\varepsilon^* \geq \varepsilon_{\min}$ (e.g., for n sufficiently large, treating A, J, M as constants), plugging $\varepsilon = \varepsilon^*$ into (10) yields the optimized rate

$$\sup_{\theta \in \Theta_{\text{BEoS}}^S(\eta, \mathcal{D})} \left| \mathbb{E}[(f_{\theta}(\mathbf{x}) - y)^2] - \widehat{R}_{\mathcal{D}}(f_{\theta}) \right| \lesssim_d A^{\alpha_A} J^{\alpha_J} M^{\alpha_M} n^{-\alpha_n}, \quad (102)$$

where

$$\alpha_A = \frac{d(d-m)}{\mathfrak{N}}, \quad \alpha_J = \frac{d(d+m)}{\mathfrak{N}}, \quad \alpha_M = \frac{4d^2}{\mathfrak{N}} + \frac{3(d+2)(d-m)(d+3)}{(2d+3)\mathfrak{N}}, \quad \alpha_n = \frac{(d-m)(d+3)}{2\mathfrak{N}}.$$

In particular, if m is fixed and $d \rightarrow \infty$, then

$$\alpha_n \rightarrow \frac{1}{6}, \quad \alpha_A \rightarrow \frac{1}{3}, \quad \alpha_J \rightarrow \frac{1}{3}, \quad \alpha_M \rightarrow \frac{11}{6},$$

so the leading-order asymptotic behavior is

$$\sup_{\theta \in \Theta_{\text{BEoS}}^S(\eta, \mathcal{D})} \left| \mathbb{E}[(f_{\theta}(\mathbf{x}) - y)^2] - \widehat{R}_{\mathcal{D}}(f_{\theta}) \right| \lesssim_d A^{\frac{1}{3}} J^{\frac{1}{3}} M^{\frac{11}{6}} n^{-\frac{1}{6}} \quad (\text{up to log factors}).$$

Proof. The optimal choice of ε minimizing the RHS of (94) is

$$\varepsilon^* \asymp A^{\frac{2d}{\mathfrak{N}}} J^{-\frac{2(2d+3)}{\mathfrak{N}}} M^{-\frac{2d(d+3)}{(2d+3)\mathfrak{N}}} n^{-\frac{d+3}{\mathfrak{N}}}, \quad (103)$$

where

$$\mathfrak{N} = (d-m)(d+3) + 2d^2 = 3d^2 + 3d - md - 3m.$$

Plugging ε^* into (94) yields

$$\begin{aligned} \sup_{\theta \in \Theta_{\text{BEoS}}^S(\eta, \mathcal{D})} \text{Gap}_{\mathcal{P}}(f_{\theta}; \mathcal{D}) &\lesssim_d A^{\frac{d(d-m)}{\mathfrak{N}}} J^{\frac{d(d+m)}{\mathfrak{N}}} M^{\frac{4d^2}{\mathfrak{N}} + \frac{3(d+2)(d-m)(d+3)}{(2d+3)\mathfrak{N}}} n^{-\frac{(d-m)(d+3)}{2\mathfrak{N}}} \\ &\lesssim_{A, M, J, d} O\left(n^{-\frac{(d-m)(d+3)}{2((d-m)(d+3) + 2d^2)}}\right). \end{aligned} \quad (104)$$

In particular, when m is fixed and $d \rightarrow \infty$,

$$\frac{(d-m)(d+3)}{2((d-m)(d+3) + 2d^2)} \rightarrow \frac{1}{6}.$$

Therefore, this rate does not suffer from the curse of dimensionality when m is fixed.

Finally, we verify the validity of the plug-in choice ε^* . The validity condition (98) requires $\varepsilon^d \gtrsim_d n^{-1/2}$ (up to logarithmic factors). Since $(\varepsilon^*)^d \asymp n^{-d(d+3)/\mathfrak{N}}$ (treating A, J, M as constants), plugging (103) into (98) gives

$$n^{-\frac{d(d+3)}{\mathfrak{N}}} \gtrsim_d n^{-1/2}.$$

This requires

$$\frac{1}{2} > \frac{d(d+3)}{\mathfrak{N}} = \frac{d(d+3)}{(d-m)(d+3) + 2d^2},$$

which is equivalent to

$$(d-m)(d+3) + 2d^2 > 2d(d+3) \iff d^2 - 3d > m(d+3) \iff m < \frac{d(d-3)}{d+3}.$$

□

D. Proof of Theorem 4.3

Let $\mathcal{D} = \{(\mathbf{x}_i, y_i)\}_{i=1}^n$ be a dataset with $\mathbf{x}_i \in \mathbb{R}^d$, and let $\mathcal{S} = \{\pi_j : \mathbb{R}^d \rightarrow \mathbb{R}^m\}_{j=1}^J$ be a collection of coordinate projections (patch extractors). For each $j \in [J]$, abbreviate the extracted patch by $\mathbf{x}^{(S_j)} := \pi_j(\mathbf{x})$, and for each sample write $\mathbf{x}_i^{(S_j)} := \pi_j(\mathbf{x}_i)$.

Assume labels are uniformly bounded: $|y_i| \leq D$ for all $i \in [n]$. Define $I_{\neq 0} := \{i \in [n] : y_i \neq 0\}$.

Consider width- K two-layer locally connected ReLU models with weight sharing and Global Average Pooling (GAP),

$$f_{\boldsymbol{\theta}}(\mathbf{x}) = \sum_{k=1}^K \frac{v_k}{J} \sum_{j=1}^J \phi\left(\mathbf{w}_k^\top \mathbf{x}^{(S_j)} - b_k\right) + \beta, \quad \phi(t) = \max\{t, 0\}, \quad (105)$$

where $\mathbf{w}_k \in \mathbb{R}^m$, $b_k \in \mathbb{R}$ are the shared filter weights and bias, $v_k \in \mathbb{R}$ is the output weight, and $\beta \in \mathbb{R}$. We write $\boldsymbol{\theta} = \{(\mathbf{w}_k, b_k, v_k)\}_{k=1}^K \cup \{\beta\}$.

Theorem D.1 (Flat interpolation with width $\leq n$). *Assume that $\|\mathbf{x}_i^{(S_j)}\|_2 \leq 1$ for all $i \in [n]$, $j \in [J]$, and there exists a map $\tau : I_{\neq 0} \rightarrow [J]$ that assigns $\mathbf{p}_i := \mathbf{x}_i^{(S_{\tau(i)})}$ such that $\|\mathbf{p}_i\|_2 = 1$ and $\mathbf{p}_i \neq \mathbf{x}_\ell^{(S_j)}$ for all $(\ell, j) \neq (i, \tau(i))$. There exists a width $K \leq n$ network of the form (1) that interpolates the dataset and whose Hessian operator norm satisfies*

$$\lambda_{\max}(\nabla_{\boldsymbol{\theta}}^2 \mathcal{L}) \leq 1 + \frac{D^2 + 2/J^2}{n}. \quad (106)$$

Construction D.2. Let $K := |I_{\neq 0}| \leq n$ and index the hidden units by $k \in I_{\neq 0}$. For each $k \in I_{\neq 0}$ define the anchor patch $\mathbf{p}_k := \mathbf{x}_k^{(S_{\tau(k)})}$ and set

$$\rho_k := \max_{(\ell, j) \neq (k, \tau(k))} (\mathbf{x}_\ell^{(S_j)})^\top \mathbf{p}_k < 1, \quad b_k \in (\rho_k, 1), \quad \mathbf{w}_k := \mathbf{p}_k. \quad (107)$$

Set the output bias and output weights

$$\beta := 0, \quad v_k := \frac{J y_k}{1 - b_k}, \quad k \in I_{\neq 0}. \quad (108)$$

(Justification of $\rho_k < 1$.) According to the assumption, for any $(\ell, j) \neq (k, \tau(k))$,

$$(\mathbf{x}_\ell^{(S_j)})^\top \mathbf{p}_k \leq \|\mathbf{x}_\ell^{(S_j)}\|_2 \|\mathbf{p}_k\|_2 \leq 1.$$

If equality held then necessarily $\|\mathbf{x}_\ell^{(S_j)}\|_2 = 1$ and $\mathbf{x}_\ell^{(S_j)} = \mathbf{p}_k$, contradicting to the assumption. Hence $\rho_k < 1$.

By (107), for any sample index i and any patch index j ,

$$\mathbf{w}_k^\top \mathbf{x}_i^{(S_j)} - b_k = \begin{cases} 1 - b_k > 0, & (i, j) = (k, \tau(k)), \\ \leq \rho_k - b_k < 0, & (i, j) \neq (k, \tau(k)). \end{cases} \quad (109)$$

Thus neuron k is active on exactly one patch in the entire collection $\{\mathbf{x}_i^{(S_j)}\}_{i,j}$, namely $\mathbf{x}_k^{(S_{\tau(k)})}$, and inactive on all other patches. Using (109) and (108), at \mathbf{x}_k we have

$$f_{\boldsymbol{\theta}}(\mathbf{x}_k) = \frac{v_k}{J} \phi(1 - b_k) = \frac{v_k}{J} (1 - b_k) = y_k, \quad k \in I_{\neq 0},$$

and for $i \notin I_{\neq 0}$ all constructed units are inactive on all patches of \mathbf{x}_i , hence $f_{\boldsymbol{\theta}}(\mathbf{x}_i) = \beta = 0 = y_i$. Therefore, $f_{\boldsymbol{\theta}}(\mathbf{x}_i) = y_i$ for all $i \in [n]$.

For each constructed unit, define

$$\tilde{v}_k := \text{sign}(v_k) \in \{\pm 1\}, \quad \tilde{\mathbf{w}}_k := |v_k| \mathbf{w}_k, \quad \tilde{b}_k := |v_k| b_k. \quad (110)$$

Then for any input \mathbf{x} ,

$$\frac{\tilde{v}_k}{J} \sum_{j=1}^J \phi(\tilde{\mathbf{w}}_k^\top \mathbf{x}^{(S_j)} - \tilde{b}_k) = \frac{v_k}{J} \sum_{j=1}^J \phi(\mathbf{w}_k^\top \mathbf{x}^{(S_j)} - b_k), \quad (111)$$

so interpolation is preserved. Moreover, the activation pattern on the full patch collection is unchanged because (109) has strict inequalities and $|v_k| > 0$. At the unique active patch $(k, \tau(k))$, the (post-rescaling) pre-activation is

$$\tilde{z}_k := \tilde{\mathbf{w}}_k^\top \mathbf{x}_k^{(S_{\tau(k)})} - \tilde{b}_k = |v_k|(1 - b_k) = J|y_k| > 0, \quad |\tilde{v}_k| = 1. \quad (112)$$

In what follows we work with the reparameterized network and drop tildes for readability, implicitly assuming $|v_k| = 1$ for all $k \in I_{\neq 0}$ and

$$z_k := \mathbf{w}_k^\top \mathbf{x}_k^{(S_{\tau(k)})} - b_k = J|y_k|. \quad (113)$$

Proposition D.3. *Let θ be the model in Construction D.2 after the reparameterization (110). Then*

$$\lambda_{\max}(\nabla_{\theta}^2 \mathcal{L}) \leq 1 + \frac{D^2 + 2/J^2}{n}.$$

Proof. By direct computation, the Hessian $\nabla_{\theta}^2 \mathcal{L}$ is given by

$$\nabla_{\theta}^2 \mathcal{L} = \frac{1}{n} \sum_{i=1}^n \nabla_{\theta} f_{\theta}(\mathbf{x}_i) \nabla_{\theta} f_{\theta}(\mathbf{x}_i)^\top + \frac{1}{n} \sum_{i=1}^n (f_{\theta}(\mathbf{x}_i) - y_i) \nabla_{\theta}^2 f_{\theta}(\mathbf{x}_i). \quad (114)$$

Since the model interpolates $f_{\theta}(\mathbf{x}_i) = y_i$ for all i , we have

$$\nabla_{\theta}^2 \mathcal{L} = \frac{1}{n} \sum_{i=1}^n \nabla_{\theta} f_{\theta}(\mathbf{x}_i) \nabla_{\theta} f_{\theta}(\mathbf{x}_i)^\top. \quad (115)$$

Denote the tangent features matrix by

$$\Phi = [\nabla_{\theta} f_{\theta}(\mathbf{x}_1), \nabla_{\theta} f_{\theta}(\mathbf{x}_2), \dots, \nabla_{\theta} f_{\theta}(\mathbf{x}_n)]. \quad (116)$$

Then (115) can be written as $\nabla_{\theta}^2 \mathcal{L} = \Phi \Phi^\top / n$, and thus

$$\lambda_{\max}(\nabla_{\theta}^2 \mathcal{L}) = \max_{\gamma \in \mathbb{S}^{(m+2)K}} \frac{1}{n} \|\Phi^\top \gamma\|^2 = \max_{\mathbf{u} \in \mathbb{S}^{n-1}} \frac{1}{n} \|\Phi \mathbf{u}\|^2. \quad (117)$$

For the gate $m_k^{(S_j)}(\mathbf{x}) := \mathbb{1}\{\mathbf{w}_k^\top \mathbf{x}^{(S_j)} > b_k\}$, let $m_{k,i}^{(S_j)} := m_k^{(S_j)}(\mathbf{x}_i)$. From direct computation,

$$\begin{aligned} \frac{\partial f_{\theta}(\mathbf{x}_i)}{\partial v_k} &= \frac{1}{J} \sum_{j=1}^J m_{k,i}^{(S_j)} \cdot (\mathbf{w}_k^\top \mathbf{x}_i^{(S_j)} - b_k), & \frac{\partial f_{\theta}(\mathbf{x}_i)}{\partial \mathbf{w}_k} &= \frac{1}{J} \sum_{j=1}^J m_{k,i}^{(S_j)} \cdot v_k \cdot \mathbf{x}_i^{(S_j)}, \\ \frac{\partial f_{\theta}(\mathbf{x}_i)}{\partial b_k} &= -\frac{1}{J} \sum_{j=1}^J m_{k,i}^{(S_j)} \cdot v_k, & \frac{\partial f_{\theta}(\mathbf{x}_i)}{\partial \beta} &= 1. \end{aligned} \quad (118)$$

By the one-to-one activation property (109), each sample \mathbf{x}_i with $i \in I_{\neq 0}$ activates exactly one unit (the unit $k = i$) on exactly one patch $S_{\tau(i)}$, and samples with $i \notin I_{\neq 0}$ activate none. Hence the sample-wise gradient $\nabla_{\theta} f_{\theta}(\mathbf{x}_i)$ has support only on the parameter triplet $(\mathbf{w}_i, b_i, v_i, \beta)$ when $i \in I_{\neq 0}$, and is zero on (\mathbf{w}_k, b_k, v_k) for all k when $i \notin I_{\neq 0}$. Writing the nonzero gradient block explicitly (recall $|v_i| = 1$ after reparameterization and (113)),

$$\begin{aligned} \nabla_{(\mathbf{w}_i, b_i, v_i, \beta)} f_{\theta}(\mathbf{x}_i) &= \begin{pmatrix} \nabla_{(\mathbf{w}_i, b_i, v_i)} f_{\theta}(\mathbf{x}_i) \\ 1 \end{pmatrix}, \\ \nabla_{(\mathbf{w}_i, b_i, v_i)} f_{\theta}(\mathbf{x}_i) &= \begin{cases} \begin{pmatrix} \frac{v_i}{J} \mathbf{x}_i^{(S_{\tau(i)})} \\ -\frac{v_i}{J} \\ \frac{1}{J} (\mathbf{w}_i^\top \mathbf{x}_i^{(S_{\tau(i)})} - b_i) \end{pmatrix} = \begin{pmatrix} \frac{v_i}{J} \mathbf{x}_i^{(S_{\tau(i)})} \\ -\frac{v_i}{J} \\ |y_i| \end{pmatrix}, & (i \in I_{\neq 0}), \\ \mathbf{0}, & (i \notin I_{\neq 0}). \end{cases} \end{aligned} \quad (119)$$

Let $\mathbf{u} = (u_1, \dots, u_n) \in \mathbb{S}^{n-1}$ and plug (119) into (117). As in the fully connected case, after a row permutation (grouping neuron parameters) we obtain

$$\begin{aligned} \lambda_{\max}(\nabla_{\theta}^2 \mathcal{L}) &= \max_{\mathbf{u} \in \mathbb{S}^{n-1}} \frac{1}{n} \|\Phi \mathbf{u}\|^2 \\ &= \frac{1}{n} \max_{\mathbf{u} \in \mathbb{S}^{n-1}} \sum_{i=1}^n u_i^2 \|\nabla_{(\mathbf{w}_i, b_i, v_i)} f_{\theta}(\mathbf{x}_i)\|_2^2 + \left(\sum_{i=1}^n u_i \right)^2 \end{aligned} \quad (120)$$

$$= \frac{1}{n} \max_{\mathbf{u} \in \mathbb{S}^{n-1}} \sum_{i \in I_{\neq 0}} u_i^2 \left(\frac{1}{J^2} \|\mathbf{x}_i^{(S_{\tau(i)})}\|_2^2 + \frac{1}{J^2} + y_i^2 \right) + \left(\sum_{i=1}^n u_i \right)^2. \quad (121)$$

According to the assumption, $\|\mathbf{x}_i^{(S_{\tau(i)})}\|_2 = 1$ for all $i \in I_{\neq 0}$, and by bounded labels $y_i^2 \leq D^2$ for all i . Thus

$$\begin{aligned} \lambda_{\max}(\nabla_{\theta}^2 \mathcal{L}) &\leq \frac{1}{n} \left(\max_{i \in [n]} \left(\frac{1}{J^2} \|\mathbf{x}_i^{(S_{\tau(i)})}\|_2^2 + \frac{1}{J^2} + y_i^2 \right) + \max_{\mathbf{u} \in \mathbb{S}^{n-1}} \left(\sum_{i=1}^n u_i \right)^2 \right) \\ &\leq \frac{1}{n} \left(\frac{2}{J^2} + D^2 + n \right) = 1 + \frac{D^2 + 2/J^2}{n}. \end{aligned}$$

If we remove the output bias term β from the parameters, then the last term $(\sum_i u_i)^2$ in (120) is removed. \square

E. Experimental Details

We adopt the random-design nonparametric regression setting introduced in Section 3. Inputs x_i are drawn i.i.d. from $\text{Uniform}(S^{d-1})$, and labels are generated as $y_i = f_{\text{true}}(x_i) + \xi_i$ where $\xi_i \sim \mathcal{N}(0, \sigma^2)$ with $\sigma^2 = 1$. The ground-truth predictor f_{true} is sampled from the LCN-WS architecture with width $K_{\text{true}} = 20$. We use disjoint coordinate patches $S_j = \{(j-1)m+1, \dots, jm\}$ with patch size $m = 10$, yielding $J = d/m$ receptive fields.

Architectures We compare two overparameterized models, both with width $K = 1024$: (i) **LCN-WS**, the two-layer \mathcal{S} -connected ReLU network with weight sharing and global average pooling (GAP) defined in (1), where filters $w_k \in \mathbb{R}^m$ are shared across all J patches; and (ii) **FCN**, the fully connected specialization obtained by setting $m = d$ and $J = 1$, where $w_k \in \mathbb{R}^d$. Both use Kaiming initialization for weights and zero initialization for biases.

Setup All models are trained with full-batch gradient descent using learning rate $\eta = 0.2$ (satisfying $\eta < 2$) for 30000 epochs on the squared loss $\mathcal{L}(\theta)$. For LCN-WS, we sweep ambient dimension $d \in \{100, 200, 400\}$; for FCN, we fix $d = 10$ as a baseline where fully connected networks are expected to perform well. Sample sizes range over $n \in \{128, 256, 512, 1024\}$. Results averaged over 5 seeds.

Table 1. Generalization gap and excess risk for LCN-WS on spherical data (corresponding to Figure 2a). As ambient dimension d increases with fixed patch size m , both metrics decrease—confirming the “blessing of dimensionality”.

d	J	Gen Gap	Excess Risk
100	10	1.283 ± 0.114	0.613 ± 0.101
200	20	0.780 ± 0.076	0.352 ± 0.047
400	40	0.295 ± 0.004	0.147 ± 0.010

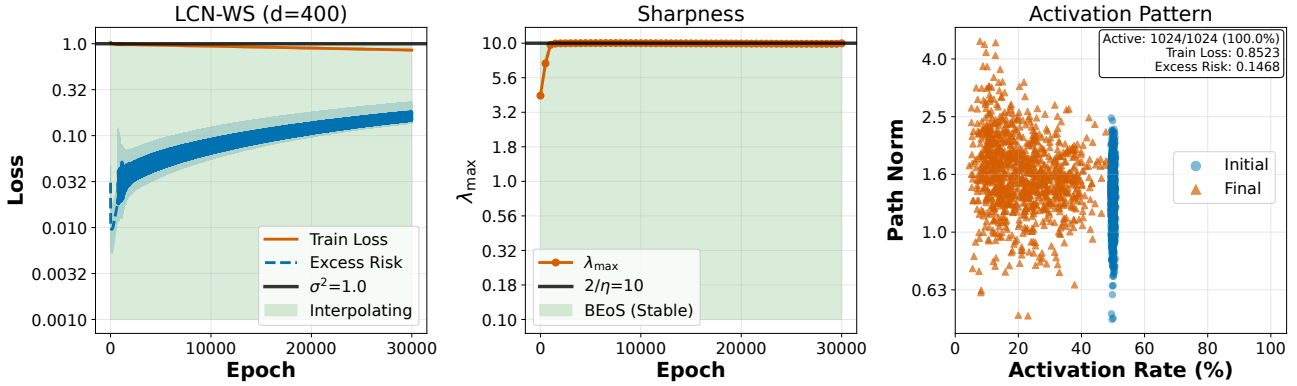


Figure 7. **LCN-WS generalizes on high-dimensional spherical data.**(Left) With $d = 400$ and fixed patch size $m \ll d$, train loss plateaus near σ^2 while excess risk decreases to 0.15, confirming generalization rather than memorization. (Middle) Sharpness saturates at BEoS ($\lambda_{\max} \approx 2/\eta$). (Right) Neurons spread across moderate activation rates, unlike the sparse isolation in flat interpolation (Figure 3). This validates Theorem 4.3: when $m \ll d$, stability-induced regularization prevents overfitting. Results averaged over 5 seeds with $\eta = 0.2$, trained for 30k epochs.

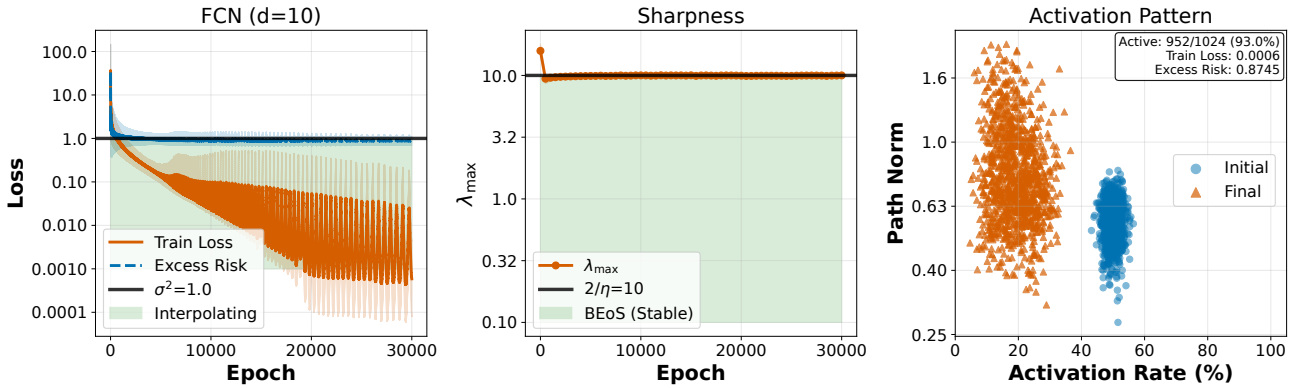


Figure 8. **FCN satisfies BEoS but still memorizes** (Left) FCN ($d = 10$) interpolates noisy labels (train loss $\rightarrow 0$) while excess risk remains $\approx \sigma^2$. (Middle) Sharpness saturates at BEoS. (Right) Activation pattern after training. Despite satisfying BEoS, FCN fails to generalize—confirming that on spherical data, stability constraints alone are insufficient without convolutional structure. Averaged over 5 seeds; with similar setting as Figure 7